Buckling of Conventional and High-Strength Vanadium Steel Double-Angle Compression Members: Computational Parametric Study

MARK D. WEBSTER, AHMET CITIPITIOGLU, RONALD L. MAYES, MOHAMED M. TALAAT and FRANK W. KAN

ABSTRACT

High-strength, low-alloy vanadium (HSLA-V) steel offers higher strength and toughness than conventional steel. The resulting lighter weight and more slender structural components are more susceptible to buckling in compression. A series of conventional Grade 50 steel and HSLA-V (nominal Grade 80) steel angle compression components was tested at Lehigh University's ATLSS laboratory. This experimental database was used to develop and verify a modeling approach using the general-purpose finite element (FE) software ABAQUS to simulate the component buckling response.

This study extensively evaluates the 2010 American Institute of Steel Construction (AISC) and Steel Joist Institute (SJI) design equations for double-angle buckling, resulting in significant findings and recommendations for both specifications. The primary objective of this paper was to assess the validity of applying the buckling equations given in the SJI 2010 Design Specification for long-span and deep-long-span joists (SJI, 2010) to double-angle compression members manufactured using 80-ksi HSLA-V steel. Present SJI specifications are applicable only for steel with specified yield stress of 50 ksi or less. Another objective of this study was to compare the design equations for compression buckling in the SJI Design Specification and the AISC 2010 *Specification* (AISC, 2010) and to develop recommendations for enhancing the accuracy of buckling equations commonly used in current practice. To achieve these goals, an extensive database of analytical buckling simulations was created to compare the performance of the code buckling equations in determining the buckling strength for regular and HSLA-V steel compression members.

Potential solutions for resolving the observed lack of conservatism in the strong-axis buckling predictions were investigated. The use of the modified component slenderness ratio in the AISC provisions significantly improved the accuracy of the SJI buckling strength predictions for strong-axis buckling cases with Q-factor values less than 1.0.

Keywords: high-strength vanadium steel, compression, computational parametric study, modification factors, buckling analysis.

INTRODUCTION

A long-term research project sponsored by the Army Research Laboratory (ARL) under Cooperative Agreement DAAD 19-03-2-0036 and executed by the Advanced Technology Institute (ATI) was initiated in 2003 to assess the impact of high-strength, low-alloy microalloyed vanadium (HSLA-V) steels on a wide variety of different applications. HSLA-V steels have specified yield strengths as high as 90 ksi and thus provide the opportunity both for weight reduction and enhanced sustainabiltiy.

This paper presents results from a computational correlation and parametric study the authors performed on double-angle compression components (SGH, 2011, 2012). A previous correlation study describes the successful use of nonlinear analytical modeling to closely match failure modes and strengths observed in 20 compression tests of double-angle members with a range of properties (SGH, 2011). Based on the success of the correlation study, the parametric study was performed to extend our findings beyond the range of parameters included in the experimental test program.

The primary objective of this parametric study is to assess the validity of applying the buckling equations given in the 2010 Steel Joist Institute (SJI) Design Specification for long-span and deep-long-span joists (SJI, 2010) to double-angle compression members manufactured using 80-ksi HSLA-V steel. Present SJI specifications are applicable only for

Mark D. Webster, Senior Structural Engineer, Simpson Gumpertz & Heger Inc., Waltham, MA. Email: MDWebster@sgh.com (corresponding)

Ahmet Citipitioglu, Director of Engineering and Design, TAV Construction, İstanbul, Turkey. Email: Ahmet.Citipitioglu@tav.aero

Ronald L. Mayes, Staff Consultant, Simpson Gumpertz & Heger Inc., San Francisco. Email: RLMayes@sgh.com

Mohamed M. Talaat, Adjunct Assistant Professor, Cairo University, Egypt and Senior Structural Engineer, Simpson Gumpertz & Heger Inc., Newport Beach, CA. Email: MTalaat@sgh.com

Frank W. Kan, Principal, Simpson Gumpertz & Heger Inc., Waltham, MA. Email: FWKan@sgh.com

Paper No. 2016-13

steel with specified yield stress of 50 ksi or less. The 2010 SJI Specification is based on the 2010 AISC *Specification* (AISC, 2010) but omits flexural-torsional buckling and the application of the slenderness modification ratio for built-up members, both of which are included in the AISC *Specification*. Another objective of this study is, therefore, to assess whether these particular AISC provisions are applicable to the design of double-angle compression members in general.

SJI long-span joists typically have double-angle top and bottom chords and single- or double-angle web members. SJI classifies steel joists into several design categories, each with its own specification. The long-span LH and DLH series share the same specification. LH-series joists commonly range in span from 25 to 95 feet, while the DLH-series can reach lengths of more than 140 feet. These joists are used for both floor and roof applications and typically support steel deck with or without concrete topping.

This paper describes the establishment of an extensive database of analytical buckling simulations covering a wide range of section parameters to compare the performance of the code buckling equations in determining the buckling strength for regular and HSLA-V steel compression members.

DESIGN FOR BUCKLING

The estimation of the critical buckling load depends on the mode and type of buckling (i.e., elastic or inelastic). The critical buckling load is computed for several possible buckling modes depending on the compression member profile. The lowest critical load for the associated buckling mode is assumed to represent the governing buckling phenomenon. The 2010 SJI Specification mostly follows the 2010 AISC *Specification* but makes some important modifications, which we discuss in this section.

Flexural Buckling

The classical buckling equation defining elastic flexural buckling, also known as Euler buckling, is used to determine the critical stress after which instability in the compression member occurs, causing it to lose its strength. This relationship, given here, is valid for slender members:

$$F_{e,i} = \frac{\pi^2 E}{(KL/r)_i^2} \tag{1}$$

where F_e is the theoretical elastic buckling stress, E is the material's Young's modulus of elasticity, L is the length of the compression member, and r is the radius of gyration of the cross-section. Subscript i refers to the two buckling axes: strong and weak axis.

A particular focus in the development of buckling equations has been the transition curve between elastic buckling and full-section yielding, which accounts for the effects of residual stresses and imperfections. Figure 1 illustrates a comparison from published literature (Salmon and Johnson, 1990) between experimental tests and critical load estimates using the AISC equations for flexural buckling of I-shape columns. The figure suggests that a larger spread of experimental results from the analytical prediction takes place at lower slenderness ratios, where inelastic buckling dominates.

The critical stress for flexural buckling given in both the SJI and AISC specifications is as follows:

$$F_{cr} = \begin{cases} \left(0.658^{\frac{QF_y}{F_{e,i}}}\right) QF_y & (KL/r)_i \le 4.71\sqrt{\dfrac{E}{QF_y}}\ ,\ \dfrac{QFy}{F_e} \le 2.25 \\ \\ 0.877 F_{e,i} & (KL/r)_i > 4.71\sqrt{\dfrac{E}{QF_y}}\ ,\ \dfrac{QFy}{F_e} > 2.25 \end{cases} \tag{2}$$

where F_{cr} is the critical buckling stress, Q is the slenderness reduction factor for unstiffened elements, and $KL/r = 4.71\sqrt{E/QF_y}$ is the demarcating slenderness ratio between elastic and inelastic buckling.

Equation 2 lists as equivalent alternatives a condition on the slenderness ratio KL/r and another condition on the critical elastic stress $QF_y/F_e = 2.25$. On closer examination, the equivalence of both limits only holds unconditionally for purely flexural buckling.

The flexural buckling equation is applied about both profile axes, and the lower critical buckling stress governs.

Modified Flexural Buckling for Built-Up Sections

The slenderness term may be modified if the buckling mode of a compression member built up from two or more shapes interconnected by bolted or welded elements is subject to relative displacement due to shear forces in the connectors between the individual shapes forming the member. For double angles with welded spacers, the AISC *Specification* modifies the slenderness ratio as follows:

$$\text{For } \frac{a}{r_i} \le 40 \qquad (KL/r)_{y,m} = (KL/r)_o \tag{3}$$

$$\text{For } \frac{a}{r_i} > 40 \qquad (KL/r)_{y,m} = \sqrt{(KL/r)_o^2 + (K_i a/r_i)^2} \tag{4}$$

where $(KL/r)_{y,m}$ is the modified slenderness ratio of the built-up member, $(KL/r)_o$ is the slenderness ratio of the built-up member acting as a unit, $K_i = 0.50$ for back-to-back angles, a is the connector spacing along the length of the member, and r_i is the minimum radius of gyration of an individual component.

This modification addresses the ability of the built-up section to act compositely in the direction(s) where the radius of gyration of a single element is significantly less than the composite value (Aslani and Goel, 1991). In the case of double-angle compression members, this modification applies only to strong-axis buckling because there is no spacer influence in the weak-axis buckling case.

Flexural-Torsional Buckling

The critical flexural-torsional buckling stress, $F_{cr,ft}$, for singly symmetric compression members—for example, double angles—without slender elements is given in the 2010 AISC *Specification* as follows. This relationship is valid for members with both compact and noncompact sections.

$$F_{cr,ft} = \frac{F_{cr,y} + F_{cr,z}}{2H}\left(1 - \sqrt{1 - \frac{4HF_{cr,y}F_{cr,z}}{\left(F_{cr,y} + F_{cr,z}\right)^2}}\right) \tag{5}$$

Slender leg elements are defined as those with width-to-thickness ratio, $b/t < 0.45\sqrt{E/F_y}$. For double angles, the relationship for this mixed-mode buckling in Equation 5 combines the strong axis flexural buckling stress, $F_{cr,y}$, given in Equation 2 and the pure torsional buckling stress, $F_{cr,z}$, given in Equation 6. The other terms used in Equation 5 are defined as follows:

$$F_{cr,z} = \frac{JG}{Ar_o^2} \tag{6}$$

$$H = 1 - \frac{x_o^2 + y_o^2}{r_o^2} \tag{7}$$

$$J = At^3/3 \tag{8}$$

where J is the torsional moment of inertia, A is the double-angle area, t is the angle leg thickness, G is the shear modulus of elasticity, r_o is the polar radius of gyration about the double-angle section's shear center, and x_o and y_o are the distances from the composite centroid to the angle shear center.

For double-angle members with slender elements, Equation 5 does not apply. Instead, Equation 2 is used where subscript i is ft, and the following modification:

$$F_{e,ft} = \frac{F_{e,y} + F_{e,z}}{2H}\left(1 - \sqrt{1 - \frac{4HF_{e,y}F_{e,z}}{\left(F_{e,y} + F_{e,z}\right)^2}}\right) \tag{9}$$

with $F_{e,z} = F_{cr,z}$ according to Equation 6 and $F_{e,y}$ according to Equation 1.

Single-Angle Buckling

Flexural buckling about the angle minor principal axis, r_z, of the individual angles forming a double-angle compression

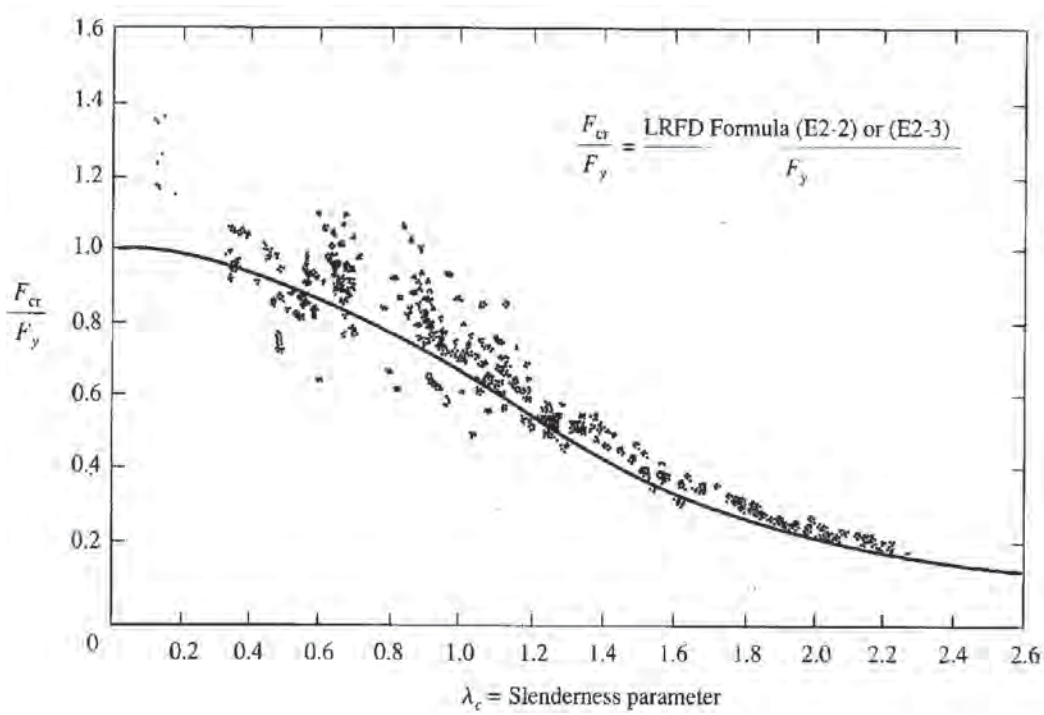

Fig. 1. Comparison of I-beam compression tests with AISC flexural buckling equations (Salmon and Johnson, 1990).

member is checked using Equation 2. Using a K factor of 1.0 implying pin-pin boundary conditions is conservative; a lower value is more realistic. This check must be performed when using both the AISC and SJI specifications.

Difference between AISC and SJI Specification Buckling Calculations

The 2010 SJI Specification considers only the flexural buckling modes of the individual angle components and the overall double-angle section, including the element slenderness reduction factor Q, which accounts for local buckling. The component slenderness modification for built-up sections and the flexural-torsional buckling mode that are a part of the AISC requirements are not considered in the SJI Specification. These additional checks in the AISC *Specification* result in more conservative design strengths, especially for double angles with low slenderness ratios (KL/r), which are common in the chord members of open web joists.

The difference among the various strong-axis buckling load strengths plotted against varying slenderness ratios for a given double-angle section geometry is shown in Figure 2. These curves are calculated for the member end conditions pinned about the strong axis and fixed about the weak axis and the two angles connected by a single spacer element. The following buckling modes are calculated:

- Sum of the buckling strength of the individual single angles between spacers, $P_{cr\text{-}flex\ z}$.
- Global double-angle flexural buckling about both weak and strong axis, $P_{cr\text{-}flex\ x}$ and $P_{cr\text{-}flex\ y}$.
- Flexural-torsional buckling, $P_{cr\text{-}flex\ tor}$.
- Flexural buckling with the modified member slenderness ratio which accounts for the influence of the connector between the angles per the AISC *Specification*, $P_{cr\text{-}flex\ y\ mod}$.

The solid red line represents the AISC lower-bound nominal strength envelope bounding all five buckling modes. Among these buckling strength curves, the dashed green line represents the strong-axis flexural buckling mode constituting the lower bound of modes considered by the SJI Specification.

PAST RESEARCH

While the behavior of single-angle compression members has been studied extensively (Kennedy and Murty, 1982; Chuenmei, 1984; Elgaaly et al., 1991; Elgaaly et al., 1992; Galambos, 1991; Popovic et al., 1999), there is less research in the literature related to double-angle compression members.

Kennedy and Murty (1972) performed compression tests of single-angle, double-angle, and tee members. The tests included six sets of three equal-leg double-angle tests with pinned ends and six sets of three double-angle tests with fixed ends. The Q factors for these tests, calculated using the current AISC *Specification*, ranged from 0.58 to 0.92, and the slenderness ratios from 22 to 90. The research found that for members with low slenderness ratios flexural-torsional buckling equations produced better results than the flexural buckling equations.

Kitipornchai and Lee (1986) performed compression tests of single-angle, double-angle, and tee pin-ended members. The tests included six sets of two equal-leg double-angle

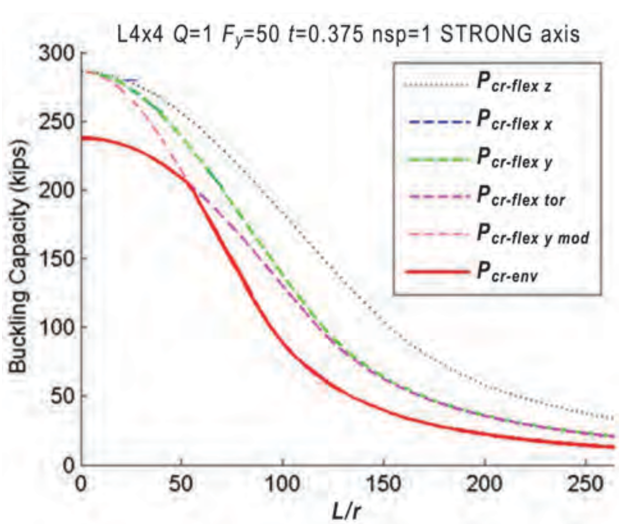

(a)

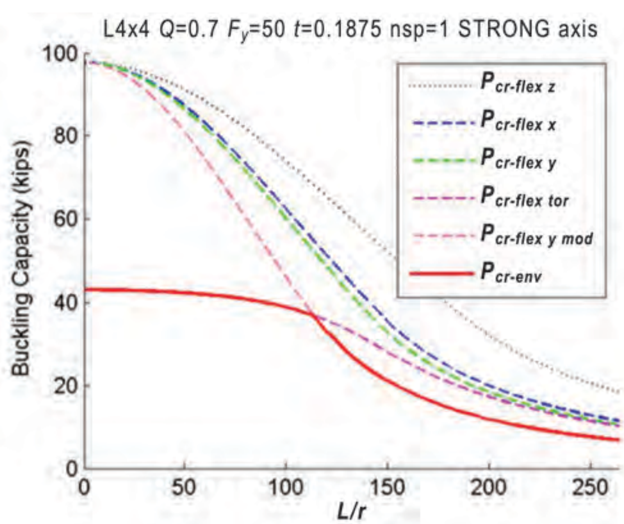

(b)

Fig. 2. Example AISC and SJI nominal buckling strength curves of different buckling modes for double-angle compression members: (a) 2L4×4×3/8 – Q = 1; (b) 2L4×4×3/16 – Q = 0.7.

Table 1. Variable Matrix of the Double-Angle Compression Member Parametric Study										
Size	L/r (based on weak axis)	F_y, ksi	Thickness t, in. $Q = 1$	$Q = 0.85$	$Q = 0.7$	Spacers	Imperfection Magnitude	End Conditions	Residual Stress, ksi	Total Cases
2L8×8	20, 40, 80, 160	50 65 80	¾ ⅞ 15⁄16	½ 9⁄16 ⅝	— — —	1, 2 bars	L/500, L/1500	Weak, strong	0	192
2L6×6	20, 40, 60, 80, 100, 160	50 65 80	9⁄16 11⁄16 ¾	⅜ 7⁄16 ½	— — —	1, 2 bars	L/500, L/1500	Weak, strong	0	288
2L4×4	50, 70, 90, 130, 150, 240	50 65 80	⅜ 7⁄16 15⁄32	¼ 9⁄32 5⁄16	3⁄16 7⁄32 ¼	1, 2 angles	L/500, L/1500	Weak, strong	0	432
2L2×2	50, 70, 90, 130, 150, 240	50 65 80	3⁄16 7⁄32 ¼	⅛ 5⁄32 5⁄32	3⁄32 ⅛ ⅛	1, 2 angles	L/500, L/1500	Weak, strong	0, 11	864

tests. The Q factors varied from 0.71 to 0.87 and the slenderness ratios from 53 to 75. This research found good agreement with the 1978 AISC ASD *Specification* (AISC, 1978), which did not include equations for flexural-torsional buckling.

Galambos (1991) proposed simplifying the 1986 AISC equations and replacing the Q factor with effective leg widths to address local buckling. He reported good results using test data from previous studies.

PARAMETERS ASSESSED

This parametric study consisted of a large number of analytical buckling simulations of double-angle specimens with 50, 65, and 80 ksi nominal yield strengths. The angle sizes included were LL8×8, LL6×6, LL4×4, and LL2×2. Table 1 lists the geometric variables used for each of the nominal yield strengths and angle sizes. A total of 3552 cases were analyzed. These cases included multiple simulations for each member size using initial geometric imperfection shapes generated by linear super-position of elastic mode shapes generated with both fixed-fixed and pinned-pinned boundary conditions at each end. For each specimen, the lower buckling strength result was reported, resulting in a database of 1776 buckling strengths. Figure 3 shows the axis definitions.

For each yield strength and angle size combination, the leg thicknesses of the angles were selected to approximate

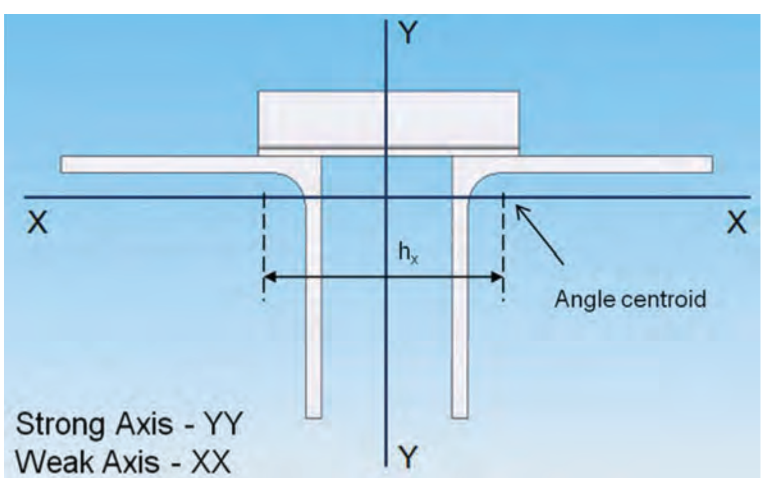

Fig. 3. Definition of local axes in double-angle member cross-sections.

the assigned element slenderness, Q, in the matrix. For the larger double-angle sizes, thicknesses were selected to produce Q factors of 1.0 and 0.85, while for the smaller angles, Q factors of 0.7, 0.85 and 1.0 were selected. Q factors for angles are defined per the AISC *Specification* (Figure 4).

The effect of spacer type and spacing between the double angles was evaluated. The large double-angle members (i.e., LL8×8 and LL6×6) were modeled assuming that bar spacers are used with a 1-in. gap between the angles. This corresponds to the typical use of these sizes as chord members within a girder assembly. The smaller double-angle members (i.e., LL4×4 and LL2×2) were modeled assuming that angle spacers are used with a larger gap of 2 in. between the angles. This corresponds to the typical use of these sizes as web members connected to the chord member legs in girders as shown in Figure 5. The spacers were located either at the midpoint between the ends of the double angles or at the third-points (one or two spacers, respectively). Bar spacers were welded 1-in.-diameter round bars located between the back-to-back angle legs. Angle spacers were angles welded to the outstanding legs of the double angles. Figure 5 shows a typical angle spacer.

The geometrical imperfections were modeled by using superimposed buckling modeshapes and scaling the maximum out-of-straightness to the target magnitude value (either L/500 or L/1500). This procedure is more completely described in a separate study by the authors (SGH, 2011). The imperfection magnitude of L/1500 is the basis of design code buckling equations. Cases with geometric imperfection magnitudes of L/500 were included to understand the effect of larger imperfections.

For each analysis model, two sets of boundary conditions were imposed. The first set corresponded to weak-axis flexural buckling, while the second set corresponded to strong-axis flexural buckling. For the first set, the rotations about the strong axis were restrained and rotation about the weak axis was permitted at the top and bottom ends of the specimen. Opposite restraints were used for the second set, enforcing a strong-axis buckling condition. Torsional rotation was restrained at both ends in all cases. Figure 6 illustrates the weak- and strong-axis set-ups.

A previous study by the authors (SGH, 2011) found that the sensitivity of the simulated buckling strength to residual stresses is minor except in small cross-sections (LL1.75×1.75×⅛), where residual stresses decreased the buckling strength by up to 10%. In larger cross-sections (LL3×3×3⁄16 and LL3.5×3.5×⅜), the modeling of residual stresses affected the buckling load by less than 5%. For the present study, only the LL2×2 series specimens were analyzed with and without residual stresses, and the lower buckling strength was used.

MODELING APPROACH

Double-Angle Modeling Steps

The generation of the set of parametric models was automated using customized scripts and the mesh generation program Truegrid (XYZ Scientific Applications, n.d.). The buckling analyses of the double angles were carried out using the general-purpose, nonlinear, finite element (FE)

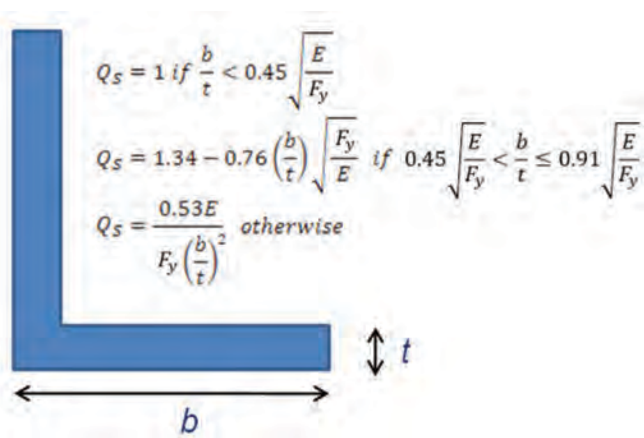

Fig. 4. Angle local element slenderness ratio.

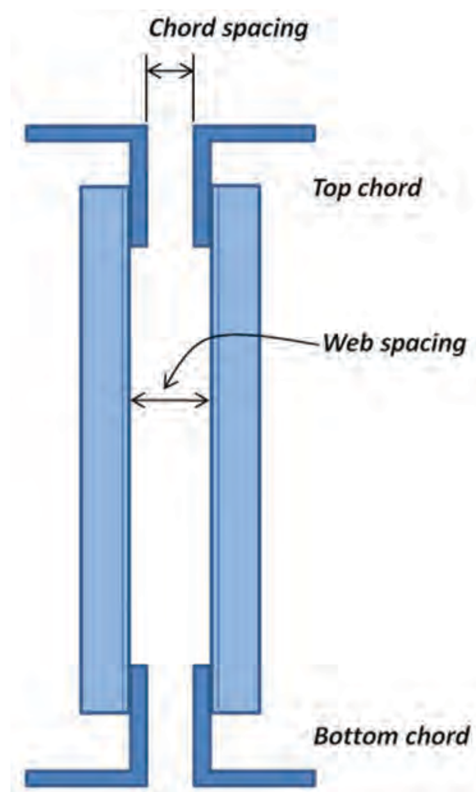

Fig. 5. Double-angle spacing definition for typical joist configuration.

software ABAQUS (2007). ABAQUS has extensive capabilities for modeling continuum mechanics, including contact, and for solving elastic buckling as well as unstable post-buckling problems. The nonlinear buckling analyses were solved using the Modified Riks algorithm, which is available in ABAQUS for loading regimes with geometrically unstable phases.

The modeling process included the following steps:

- Angles and angle spacers were modeled using four-node shell elements; eight-node continuum elements were used to model the bar spacers. A cross-section of a model is shown in Figure 7.
- To ensure conservative buckling strengths for the LL2×2 and LL4×4 double-angle members, L1×1×⅛ spacer angles were used, which are on the lighter side of standard industry practice. For the LL6×6 and LL8×8 members, 4-in.- and 5-in.-long bar spacers were used, respectively. The configurations of the spacers are shown in Figure 8.
- The material properties are shown in Figure 9.
- For LL2×2 angles, an alternate series of models were analyzed that included the effect of residual stresses. The residual stresses were imposed at the angle legs in the longitudinal direction prior to loading and allowed to equilibrate. The residual stress distribution profile across each angle leg cross-section is shown in Figure 10. A maximum residual stress magnitude of 10.8 ksi was imposed.

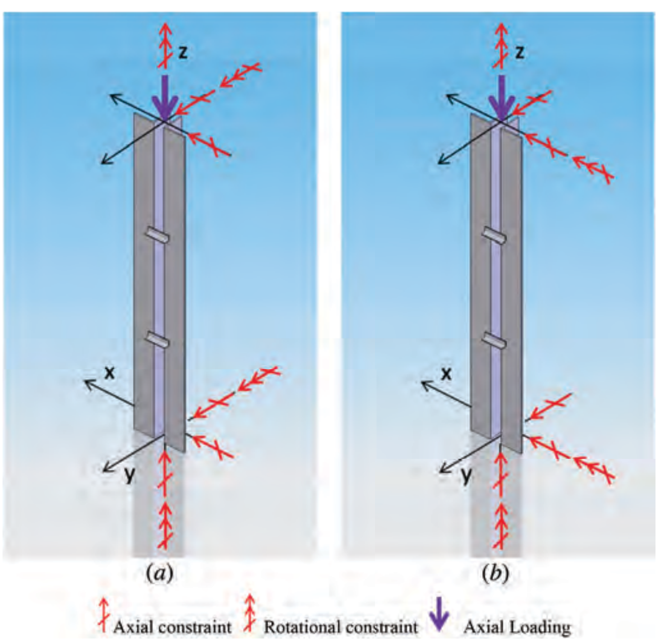

Fig. 6. Double-angle model boundary conditions for weak and strong axis buckling analyses: (a) weak-axis pinned; (b) strong-axis pinned.

- Buckling mode shapes of each specimen were determined using an elastic eigenvalue analysis for each perfect geometry model. The analyses yielded the critical loads and mode shapes for a large number of buckling modes. Initial geometric imperfections were introduced by combining a number of buckling mode shapes that fall within a given multiple of the fundamental elastic load.

ANALYSIS RESULTS

Table 2 summarizes the ratios of analysis results to the predictions of the SJI Specification for the different parameter study variables. Figures 11 through 14 show typical graphical comparisons of the analytical results to the SJI Specification. The weak-axis buckling strengths are well-predicted by the flexural buckling curve in the SJI Specification (Figures 11 and 13), while the SJI Specification overpredicts the strong-axis buckling strength (Figures 12 and 14).

Figure 15 summarizes these results for the LL4×4 analyses, sorted by Q factor and the number of spacers. For small slenderness ratios, the strong-axis results are closer to the SJI predictions, but the SJI Specification becomes increasingly nonconservative with increasing slenderness ratios.

Table 3 and Figure 16 illustrate a key finding: Across all investigated parameters, the SJI Specification predicts the buckling strength of high-strength vanadium steel (80 ksi) and conventional steel (50 ksi) equally well. The table indicates $(P_{fe}/P_{n\mathrm{SJI}})_{Fy}/(P_{fe}/P_{n\mathrm{SJI}})_{50}$, where:

$(P_{fe}/P_{n\mathrm{SJI}})_{Fy}$ = ratio of the analytical buckling strength to the strength predicted by the SJI Specification for steel with a yield stress of F_Y

$(P_{fe}/P_{n\mathrm{SJI}})_{50}$ = ratio of the analytical buckling strength to the strength predicted by the SJI Specification for steel with a yield stress of 50 ksi

The graphs provide a similar metric using the ratios of analytical to predicted buckling stress for 80-ksi and 50-ksi steel. Values of unity indicate that the equations predict the buckling strength (or stress) equally well for both yield stresses.

There is no discernible bias in these current buckling equations when used with grades representative of HSLA-V material. The overall mean value of the ratio of the ratios from Table 3 is 1.00 and 1.01 for imperfection ratios of L/1500 and L/500, respectively. This result clearly demonstrates that the overall margin of safety for the higher yield strength HSLA-V steels is the same as 50-ksi steel when considering all of the variables included in this study.

The results for weak-axis buckling show that the SJI buckling equations are adequate and appropriately conservative for almost all cases included in this study. The results for strong-axis buckling, however, show that the SJI buckling equations are nonconservative for many cases, and the

Table 2. Global Comparison of Analysis versus SJI Specification Buckling Strength Ratio							
Global Average of P_{fe}/P_{n}_SJI							
		L/1500			L/500		
Axis	**Variable**	**50 ksi**	**65 ksi**	**80 ksi**	**50 ksi**	**65 ksi**	**80 ksi**
	***Q* Factor**						
Strong	0.7	0.855	0.890	0.868	0.782	0.808	0.787
	0.85	1.033	1.034	1.021	0.900	0.916	0.917
	1	1.019	1.011	1.004	0.928	0.930	0.929
Weak	0.7	1.045	1.104	1.095	0.945	1.016	1.021
	0.85	1.186	1.172	1.160	1.066	1.083	1.080
	1	1.136	1.126	1.116	1.062	1.060	1.055
	Number of Spacers						
Strong	1	0.973	0.973	0.958	0.872	0.878	0.873
	2	1.005	1.015	1.005	0.899	0.918	0.915
Weak	1	1.124	1.127	1.116	1.030	1.050	1.043
	2	1.148	1.151	1.142	1.047	1.069	1.072
	Mean: Strong	0.989	0.994	0.982	0.886	0.898	0.894
	Mean: Weak	1.136	1.139	1.129	1.038	1.060	1.058
	Mean: Weak and strong	**1.063**	**1.067**	**1.055**	**0.962**	**0.979**	**0.976**
	Grand total	**1.061**			**0.972**		

nonconservatism increases as the Q factor decreases from 1.0 to 0.7. This nonconservatism occurs regardless of material yield stress.

To address the nonconservatism in the SJI strong-axis buckling results, the following possible modifications to the SJI Specification were investigated:

- Full adoption of the AISC *Specification* equations.
- Adoption of the AISC component slenderness (KL/r) modification equation only.
- Adoption of a revised Q factor calculation.

This paper addresses the first two options. A separate paper by the authors (Talaat et al., 2017) evaluates proposed changes to the Q factor calculation that would address the nonconservatism associated with low Q factors. It is shown that using the Q factor formulation from the 1968 AISI Specification, which accounts for twisting of the angle cross section when both legs buckle locally in the same direction, eliminates the Q factor nonconservatism seen in the results.

PROPOSED MODIFICATIONS TO THE 2010 SJI BUCKLING DESIGN EQUATIONS

A number of potential solutions for resolving the lack of conservatism in the SJI Specification's strong-axis strength predictions were investigated. Two options are addressed in this paper:

1. The adoption by SJI of all of the AISC provisions, including both the torsional flexural buckling and the slenderness modification ratio used for built-up compression members.
2. The adoption by SJI of the AISC slenderness modification ratio used for built-up compression members but not the AISC flexural-torsional provisions.

Use of All AISC Buckling Provisions

In addition to the flexural buckling modes considered by the SJI Specification, the AISC *Specification* considers the flexural-torsional buckling failure mode and modification of the slenderness ratio (KL/r) for built-up members. In the case of double angles, this modification applies only to the strong-axis buckling where the spacers affect the deformation of the overall section.

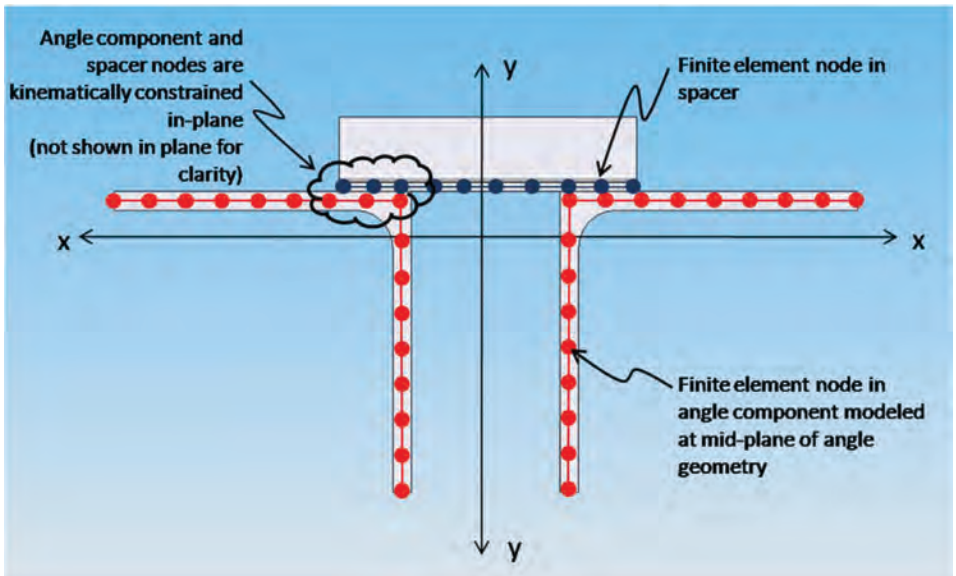

Fig. 7. Double-angle cross-section modeling scheme and constraint between angle and spacer nodes.

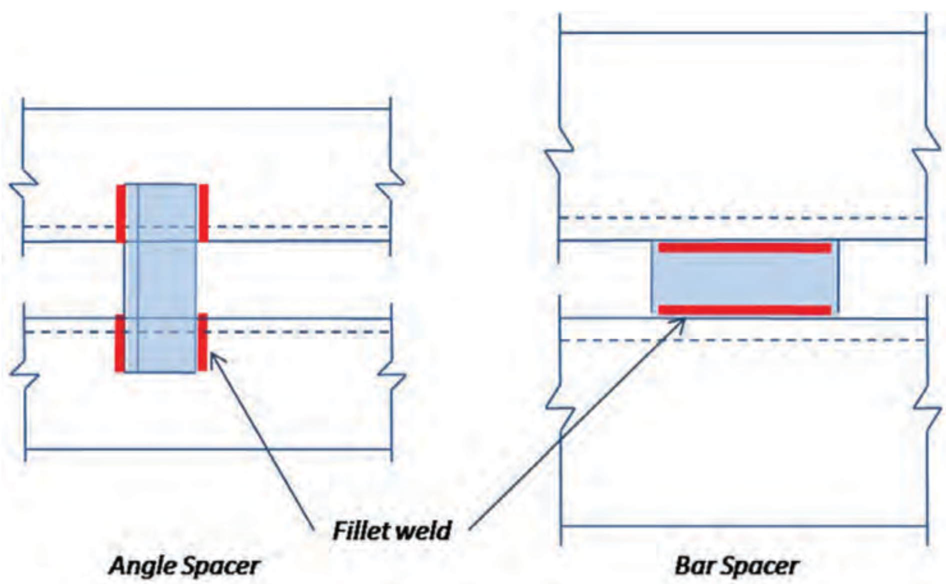

Fig. 8. Double-angle bar spacers (chord members) and angle spacers (web).

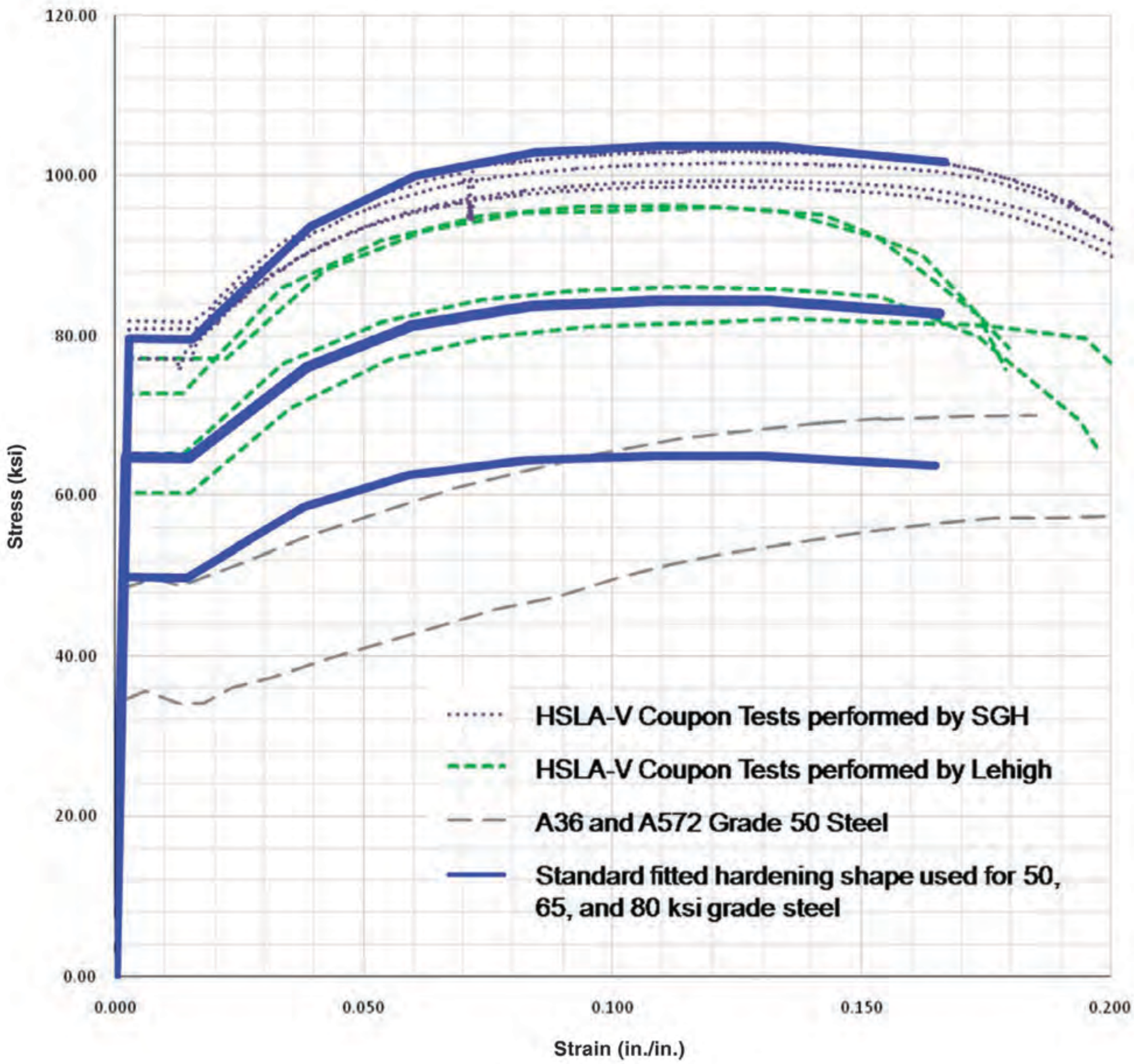

Fig. 9. Fitted hardening shapes compared to coupon tests or ASTM standard response for 50-, 65- and 80-ksi materials [ASTM A36/A 36M-08 (2008) and A 572/A 572M-07 (2007)].

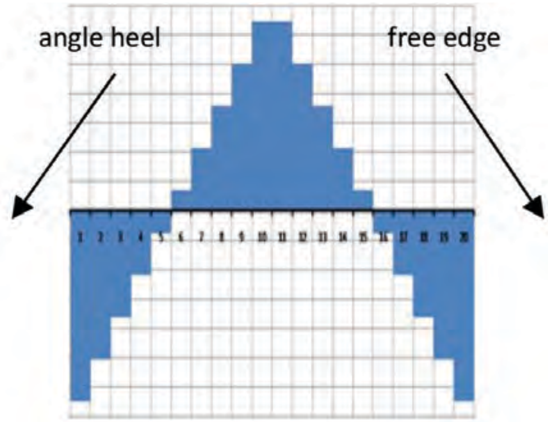

Fig. 10. Residual stress profile discretization across the angle leg.

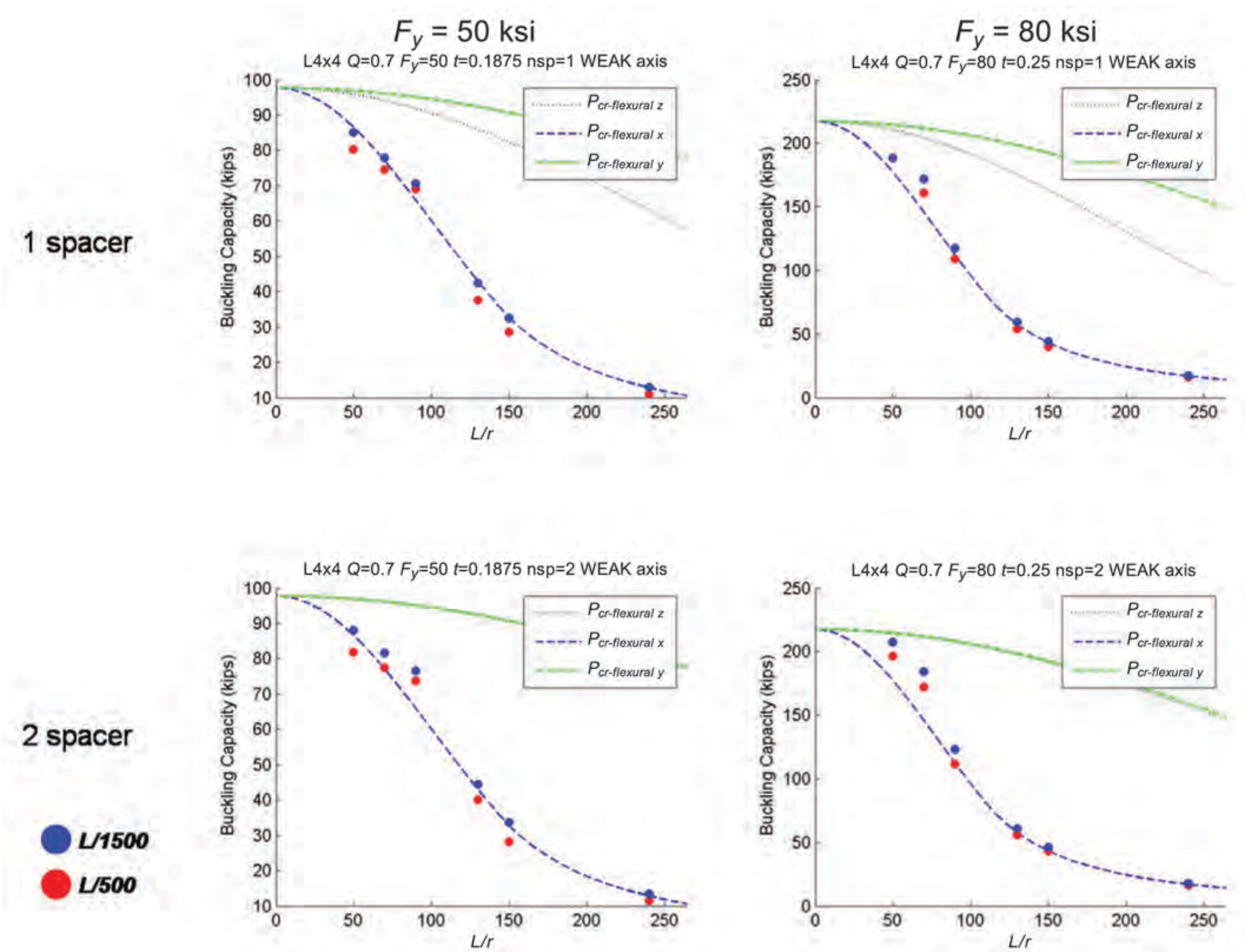

Fig. 11. LL4×4 analytical weak-axis (pinned) buckling strengths compared to the SJI Specification equations; L/500 and L/1500 imperfection magnitudes; F_y *= 50-ksi and 80-ksi materials;* Q *= 0.7.*

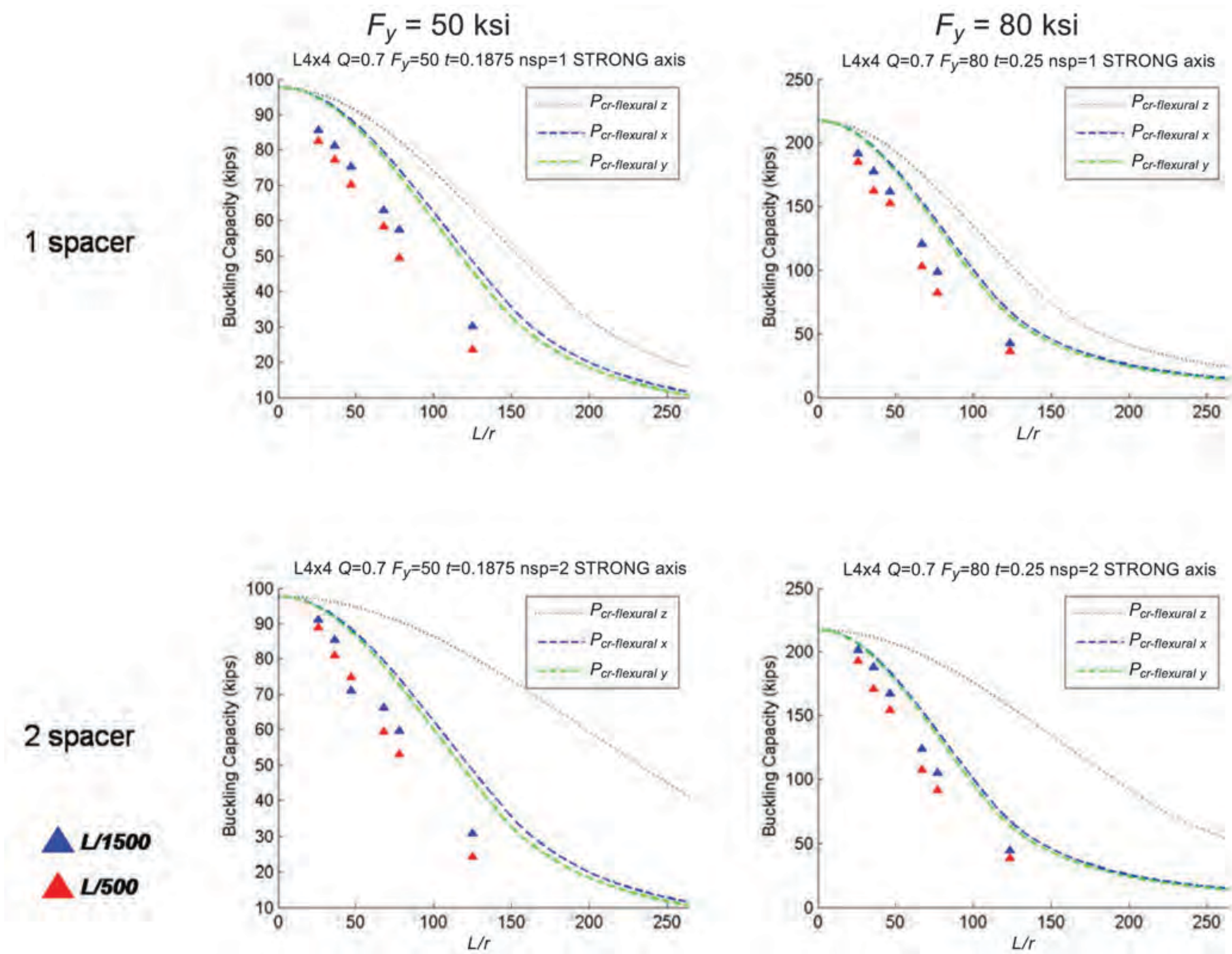

Fig. 12. LL4×4 analytical strong-axis (pinned) buckling strengths compared to the SJI Specification equations; L/500 and L/1500 imperfection magnitudes; F_y *= 50-ksi and 80-ksi materials;* Q *= 0.7.*

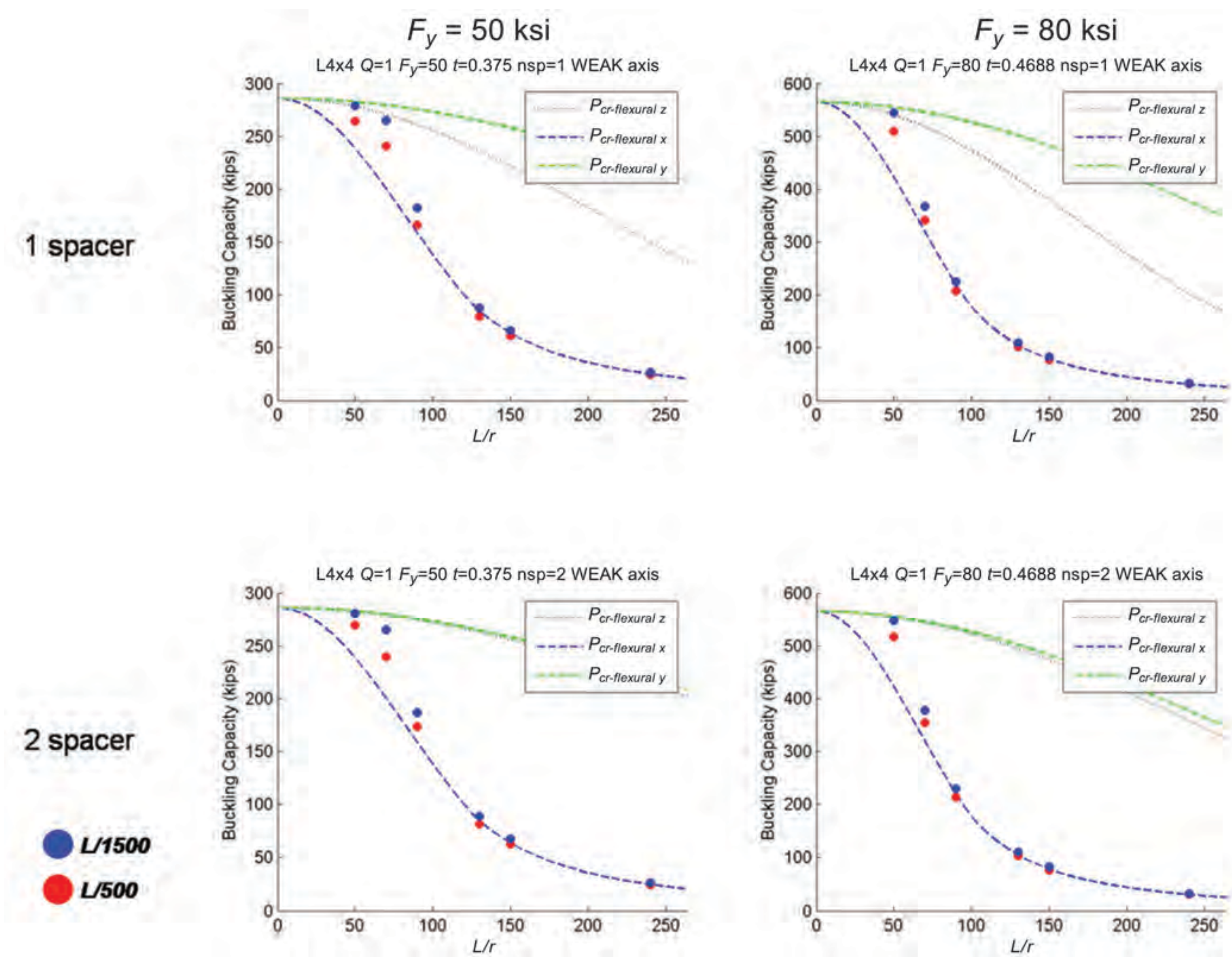

Fig. 13. LL4×4 analytical weak-axis (pinned) buckling strengths compared to the SJI Specification equations; L/500 and L/1500 imperfection magnitudes; F_y = *50-ksi and 80-ksi materials;* Q = *1.0.*

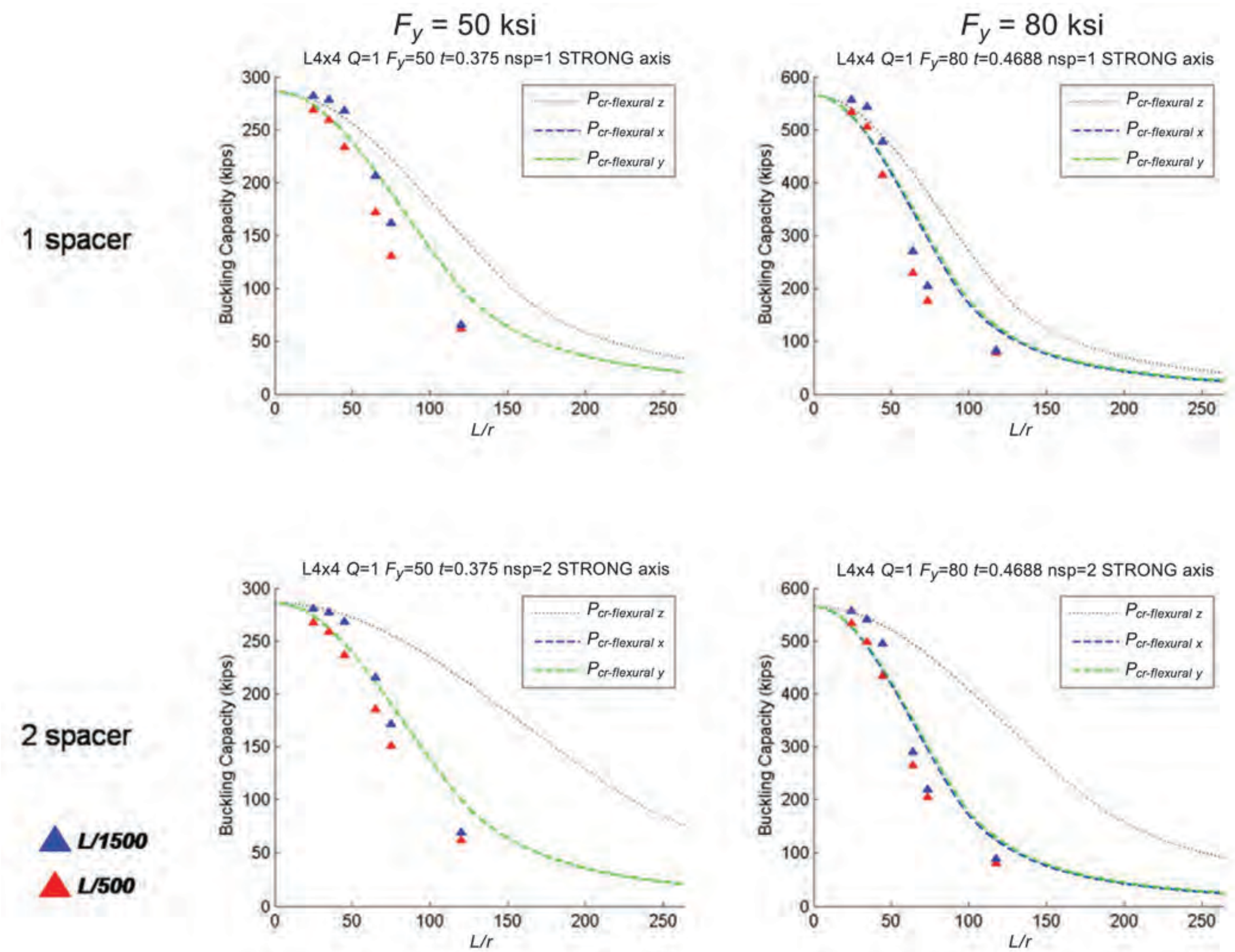

Fig. 14. LL4×4 analytical strong-axis (pinned) buckling strengths compared to the SJI Specification equations; L/500 and L/1500 imperfection magnitudes; F_y = *50-ksi and 80-ksi materials;* Q = *1.0.*

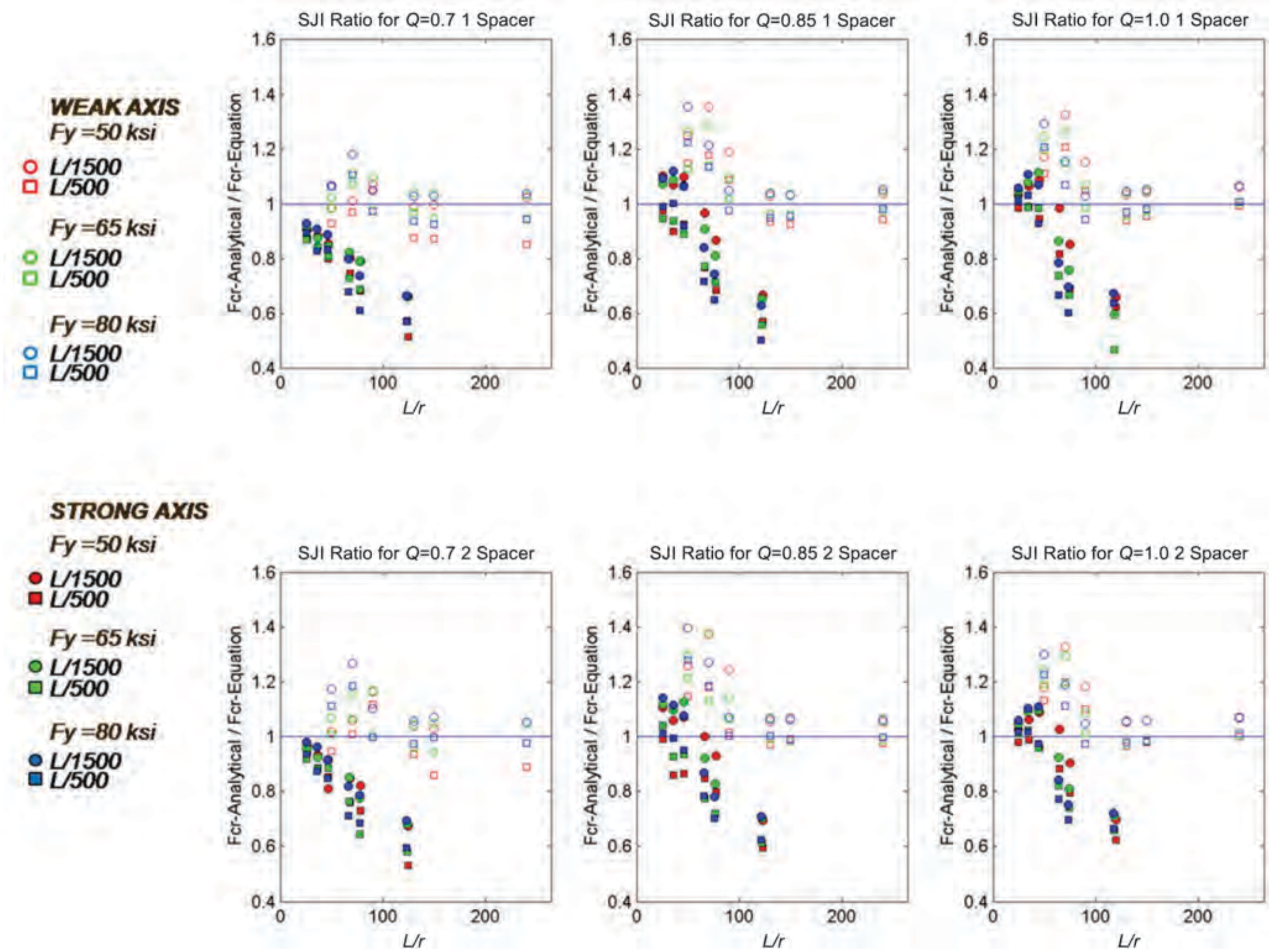

Fig. 15. LL4×4 ratios of analytical buckling strength to the SJI Specification buckling strength; L/500 and L/1500 imperfection magnitudes; F_y *= 50-, 65- and 80-ksi materials—organized per* Q *values and spacer count.*

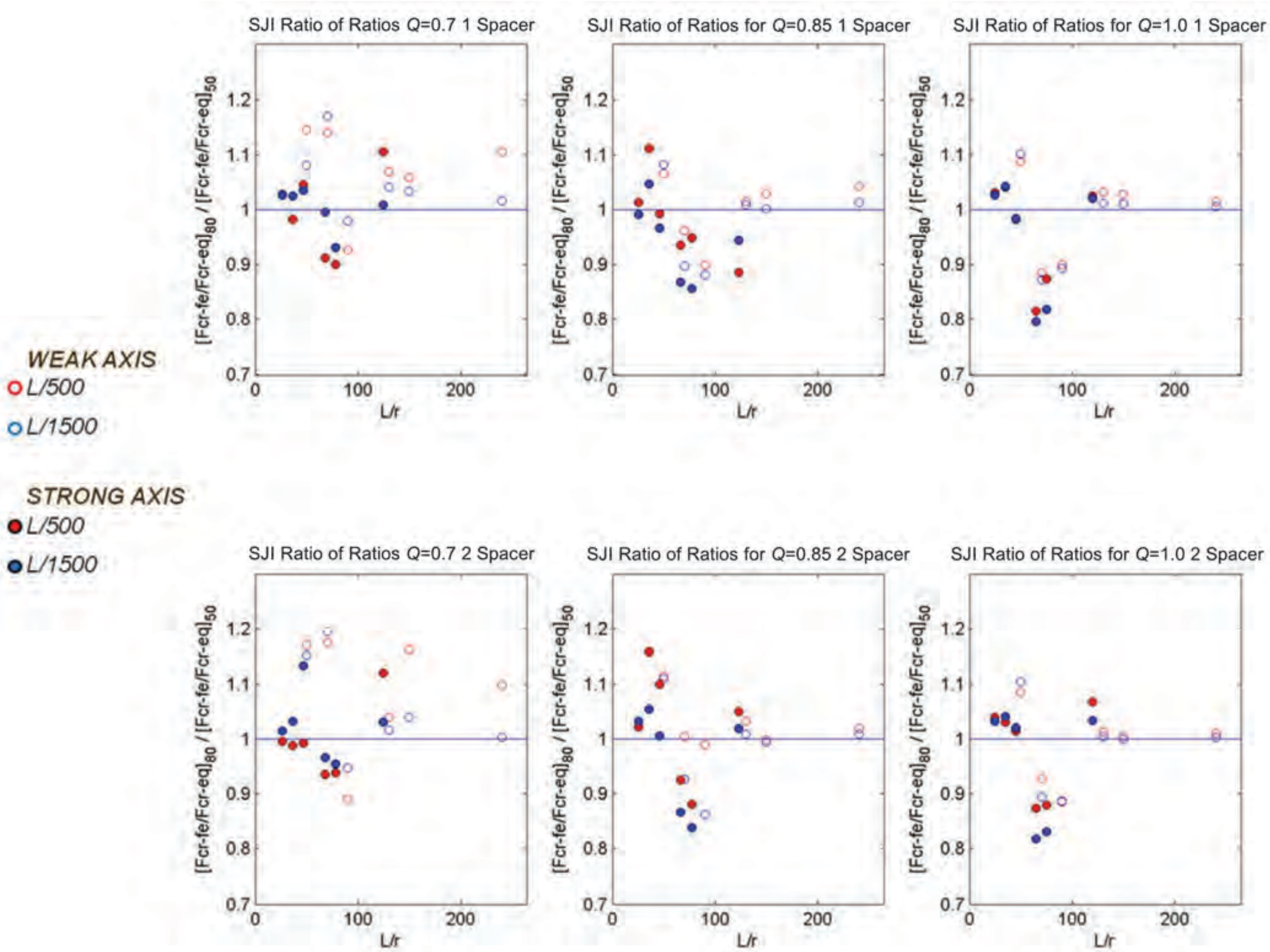

Fig. 16. LL4×4 ratio of ratios of analytical to SJI Specification buckling strength for the 80- and 50-ksi grade steel; L/500 and L/1500 imperfection magnitudes organized per Q *values and spacer count.*

Table 3. Global Comparison of Analytical to SJI Specification Buckling Strength Ratio of Ratios per Material Strength								
Global Average of $(P_{fe}/P_n\_SJI)_{Fy}/(P_{fe}/P_n\_SJI)_{50}$								
		L/1500				L/500		
Axis	**Variable**	**50 ksi**	**65 ksi**	**80 ksi**		**50 ksi**	**65 ksi**	**80 ksi**
	***Q* Factor**							
Strong	0.7	1.000	1.040	1.015		1.000	1.036	1.009
	0.85	1.000	1.000	0.986		1.000	1.017	1.017
	1	1.000	0.991	0.986		1.000	1.000	1.001
Weak	0.7	1.000	1.056	1.048		1.000	1.077	1.084
	0.85	1.000	0.989	0.981		1.000	1.017	1.014
	1	1.000	0.993	0.986		1.000	0.999	0.995
	Number of Spacers							
Strong	1	1.000	1.000	0.984		1.000	1.007	0.999
	2	1.000	1.010	1.001		1.000	1.022	1.019
Weak	1	1.000	1.005	0.997		1.000	1.022	1.016
	2	1.000	1.005	0.998		1.000	1.024	1.028
	Mean: Strong	1.000	1.005	0.992		1.000	1.014	1.009
	Mean: Weak	1.000	1.005	0.998		1.000	1.023	1.022
	Mean: Weak and strong	**1.000**	**1.005**	**0.995**		**1.000**	**1.019**	**1.015**
	Grand total	**1.000**				**1.011**		

Tables 4 and 5 and Figures 17 through 22 illustrate the results of our study using the same format used above for presentation of the SJI Specification buckling equation comparison for different material yield stress values.

It is clear from the results that the use of the AISC buckling equations solves the nonconservatism observed with the use of the SJI equations for strong-axis bending and low Q factors. However, due to the flexural-torsional buckling check, the AISC buckling equations are highly conservative for combinations of low slenderness ratio and Q factor under 1.0. Also, as seen in Table 5, the AISC equations produce less conservative nominal buckling strength predictions for higher-strength steels than for 50-ksi steel, though they are conservative even for the higher strength steels, as indicated in Table 4.

Use of AISC Modified Slenderness Ratio Provision Only

As observed, the AISC flexural-torsional buckling equation for double-angle sections results in highly conservative strength predictions in many cases. The flexural buckling equations used alone provide better predictions for compression members with low slenderness ratios.

The following tables and figures illustrate the results of SJI adopting the AISC modified slenderness ratio provisions without the flexural-torsional buckling equations. Table 6 summarizes the ratios of the analytical results to the predicted buckling strengths. This approach provides good results, except for strong-axis buckling cases with $Q = 0.7$, where the buckling strengths are overpredicted by the SJI Specification equations and are thus unconservative. However, even for these cases, this approach provides better results than the existing SJI equations that do not include the modified slenderness ratio (Figure 12 compared to Figure 18).

Figures 23 through 25 compare normalized analytical results to predicted strengths for $Q = 1.0$, 0.85 and 0.7, respectively. These graphs also include the test results from the Kennedy and Murty (1972) and Kitipornchai and Lee (1986) studies. These historical test results generally fall within the range of the parametric study results, with the exception of the Kennedy and Murty test results for specimens with low slenderness ratios and $Q = 1.0$, which, though at the lower edge of the range of our study results, still show good agreement with the predicted strengths using the AISC flexural buckling equation with the modified slenderness ratio.

Table 4. Global Comparison of Analytical to AISC *Specification* Nominal Buckling Strength Ratios (compare to Table 2)								
Global Average of P_{fe}/P_{n}_AISC								
		L/1500				**L/500**		
Axis	**Variable**	**50 ksi**	**65 ksi**	**80 ksi**		**50 ksi**	**65 ksi**	**80 ksi**
	***Q* Factor**							
Strong	0.7	2.243	1.988	1.996		2.068	1.813	1.828
	0.85	1.714	1.610	1.624		1.491	1.425	1.454
	1	1.199	1.169	1.159		1.094	1.075	1.074
Weak	0.7	1.892	1.678	1.657		1.722	1.547	1.559
	0.85	1.549	1.431	1.420		1.391	1.321	1.319
	1	1.163	1.140	1.125		1.088	1.074	1.064
	Number of Spacers							
Strong	1	1.607	1.504	1.505		1.444	1.354	1.371
	2	1.643	1.532	1.538		1.474	1.387	1.399
Weak	1	1.452	1.353	1.337		1.332	1.260	1.251
	2	1.490	1.387	1.373		1.353	1.285	1.290

Mean: Strong	1.625	1.518	1.521		1.459	1.371	1.385
Mean: Weak	1.471	1.370	1.355		1.343	1.272	1.270
Mean: Weak and strong	**1.548**	**1.444**	**1.438**		**1.401**	**1.322**	**1.328**
Grand total	**1.477**				**1.350**		

Table 7 summarizes the ratios of ratios (compare to Table 3). It is clear from these results that the three material strengths result in generally similar degrees of conservatism for the range of variables in this study. For cases where $Q = 0.7$, there is slightly more conservatism for the higher-strength material specimens.

The results show that the modified slenderness ratio in the current AISC provisions significantly improves the accuracy of the SJI buckling strength predictions for strong-axis buckling of members with Q lower than 1.0. The ratio of analytical to code buckling prediction is above unity for all but the lowest Q factor value of 0.7 and strong-axis buckling using the code-basis imperfection magnitude of L/1500. The overall means are above unity for both weak- and strong-axis buckling, and the grand total mean is 1.09. Moreover, the ratios shown in Table 7 exhibit no discernible bias based on material yield stress, which means that the proposed buckling prediction equation is equally reliable for conventional 50-ksi and HSLA-V steels when considering all of the variables included in this study.

CONCLUSIONS

This study extensively evaluates the 2010 AISC and SJI design equations for double-angle buckling, resulting in significant findings and recommendations for both specifications.

One of the primary goals of this parametric study was to determine if the 2010 SJI design equations for double-angle buckling would produce a similar margin of safety for HSLA-V and 50-ksi steels. By comparing the ratio of the analytical buckling strength to the limiting SJI buckling strength for the higher-grade steels to the ratio of the analytical buckling strength to the limiting SJI buckling strength for the base 50-ksi strength material, it was demonstrated that there is no discernible bias in the SJI current buckling equations when used with grades representative of HSLA-V material. The overall margin of safety for the higher-yield stress HSLA-V steels is the same as 50-ksi steel when considering all of the variables included in this study.

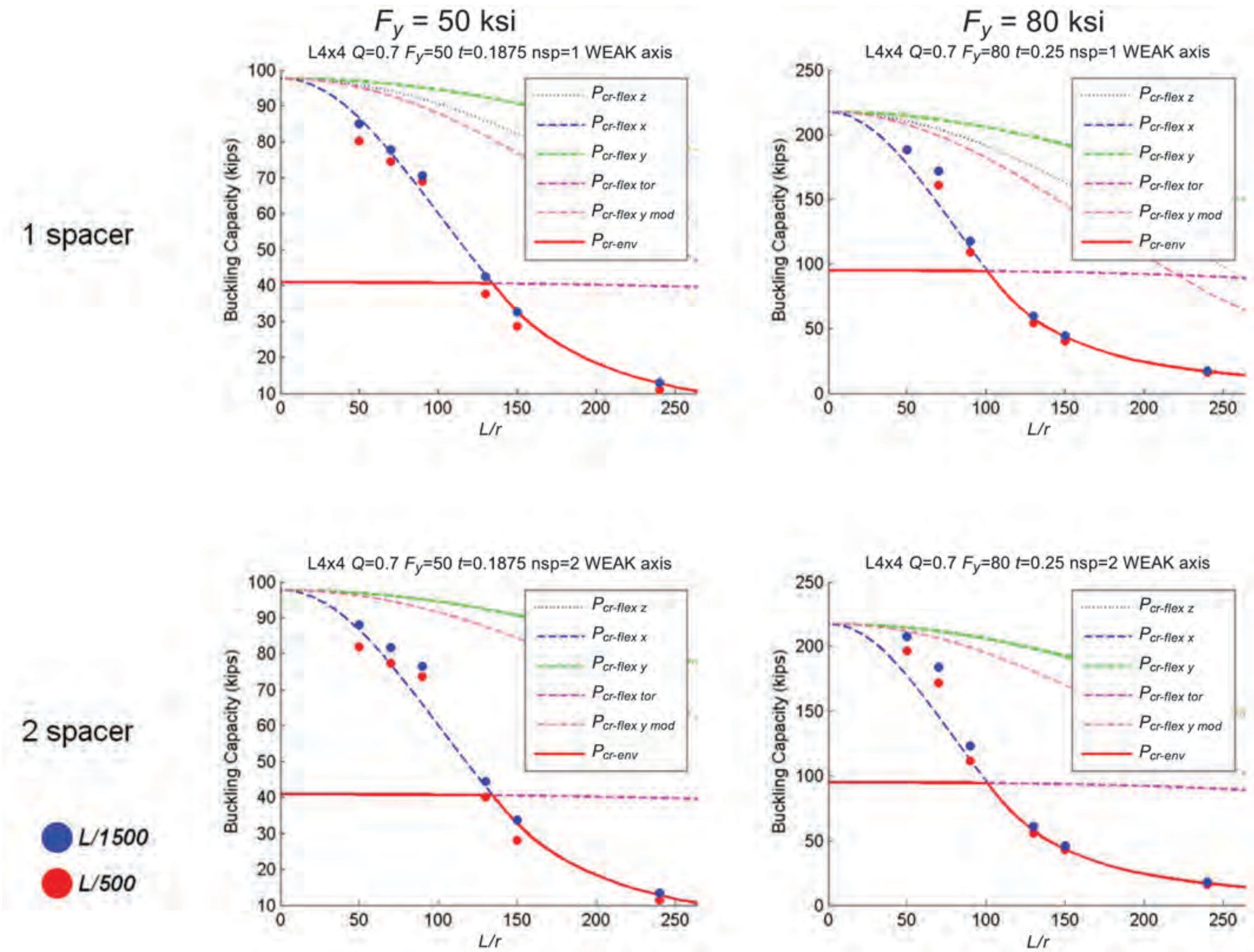

Fig. 17. LL4×4 analytical weak-axis (pinned) buckling strengths compared to AISC Specification *equations; L/500 and L/1500 imperfection magnitudes;* F_y *= 50-ksi and 80-ksi materials;* Q *= 0.7 (compare to Fig. 11).*

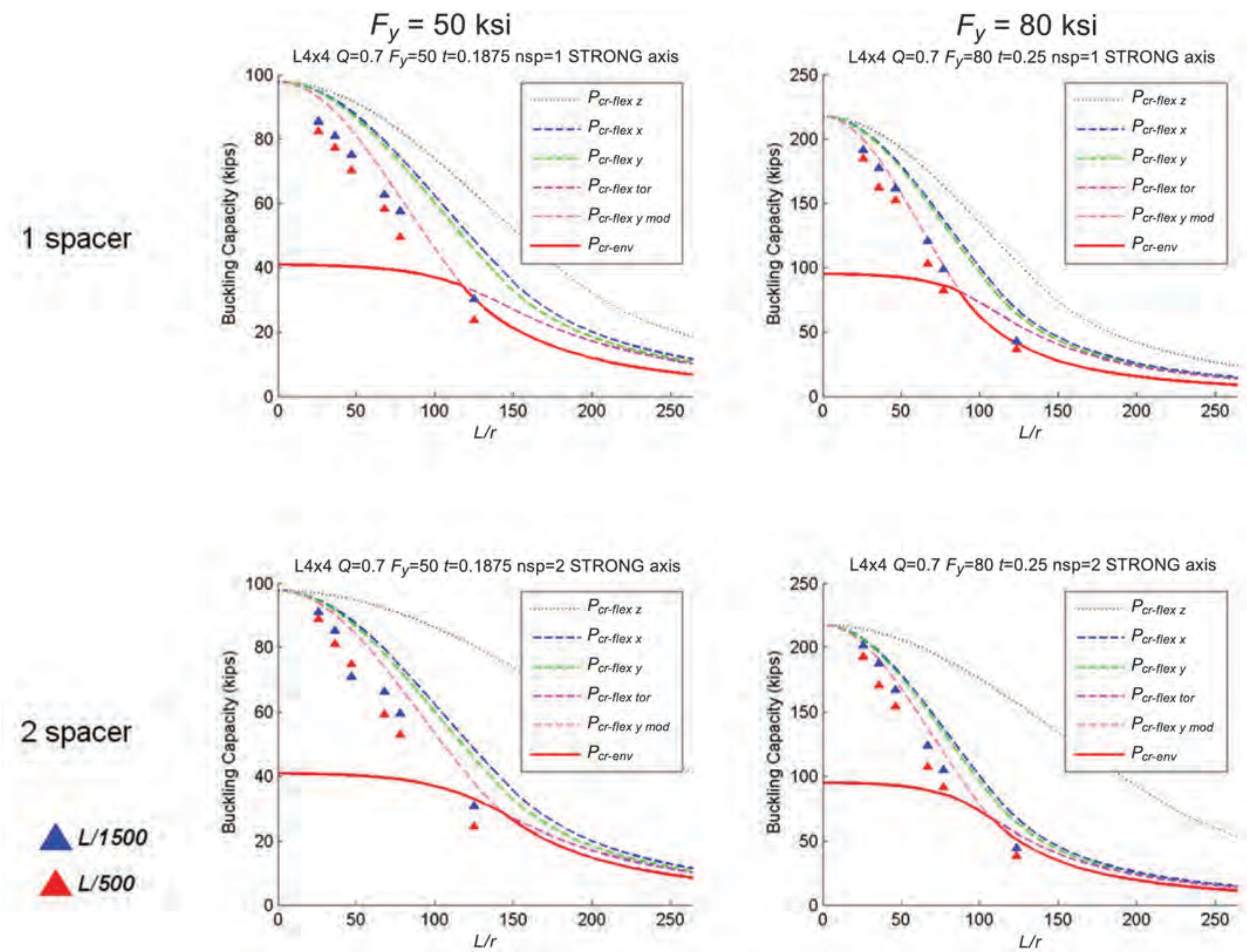

Fig. 18. LL4×4 analytical strong-axis (pinned) buckling strengths compared to AISC Specification *equations; L/500 and L/1500 imperfection magnitudes;* F_y *= 50-ksi and 80-ksi materials;* Q *= 0.7 (compare to Fig. 12).*

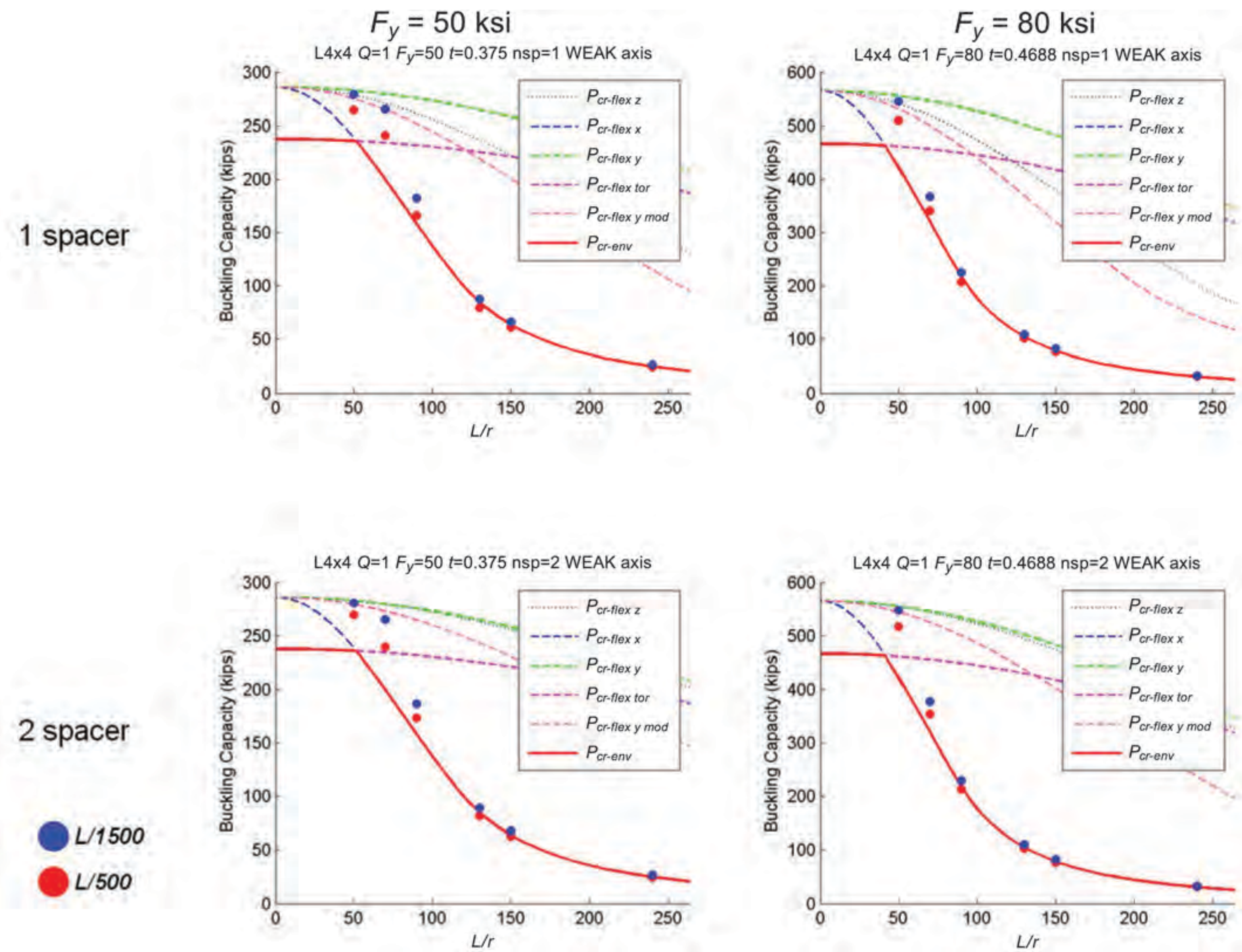

Fig. 19. LL4×4 analytical weak-axis (pinned) buckling strengths compared to AISC Specification *equations; L/500 and L/1500 imperfection magnitudes;* F_y *= 50-ksi and 80-ksi materials;* Q = *1.0 (compare to Fig. 13).*

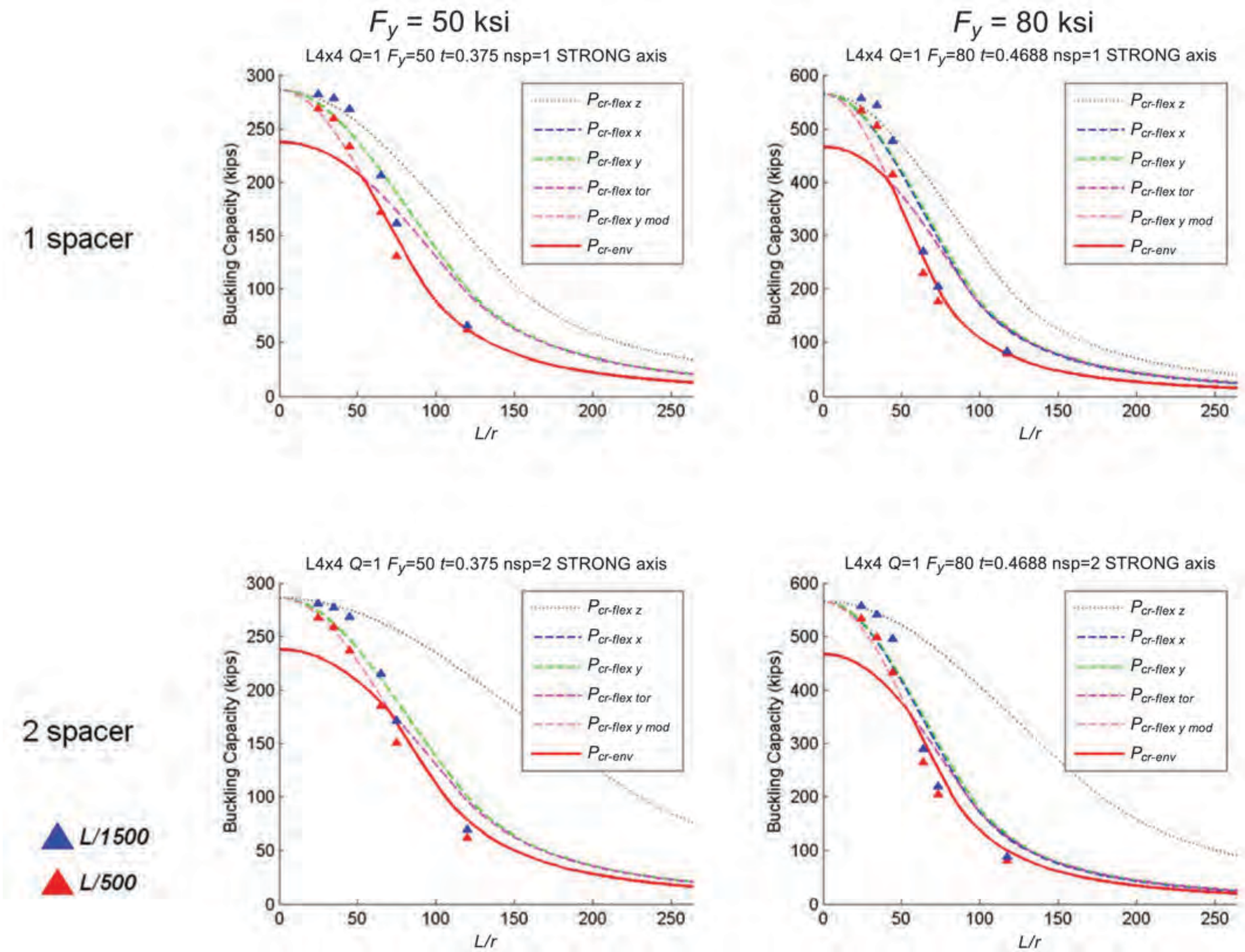

Fig. 20. LL4×4 analytical strong-axis (pinned) buckling strengths compared to AISC Specification *equations; L/500 and L/1500 imperfection magnitudes;* F_y *= 50-ksi and 80-ksi materials;* Q = *1.0 (compare to Fig. 14).*

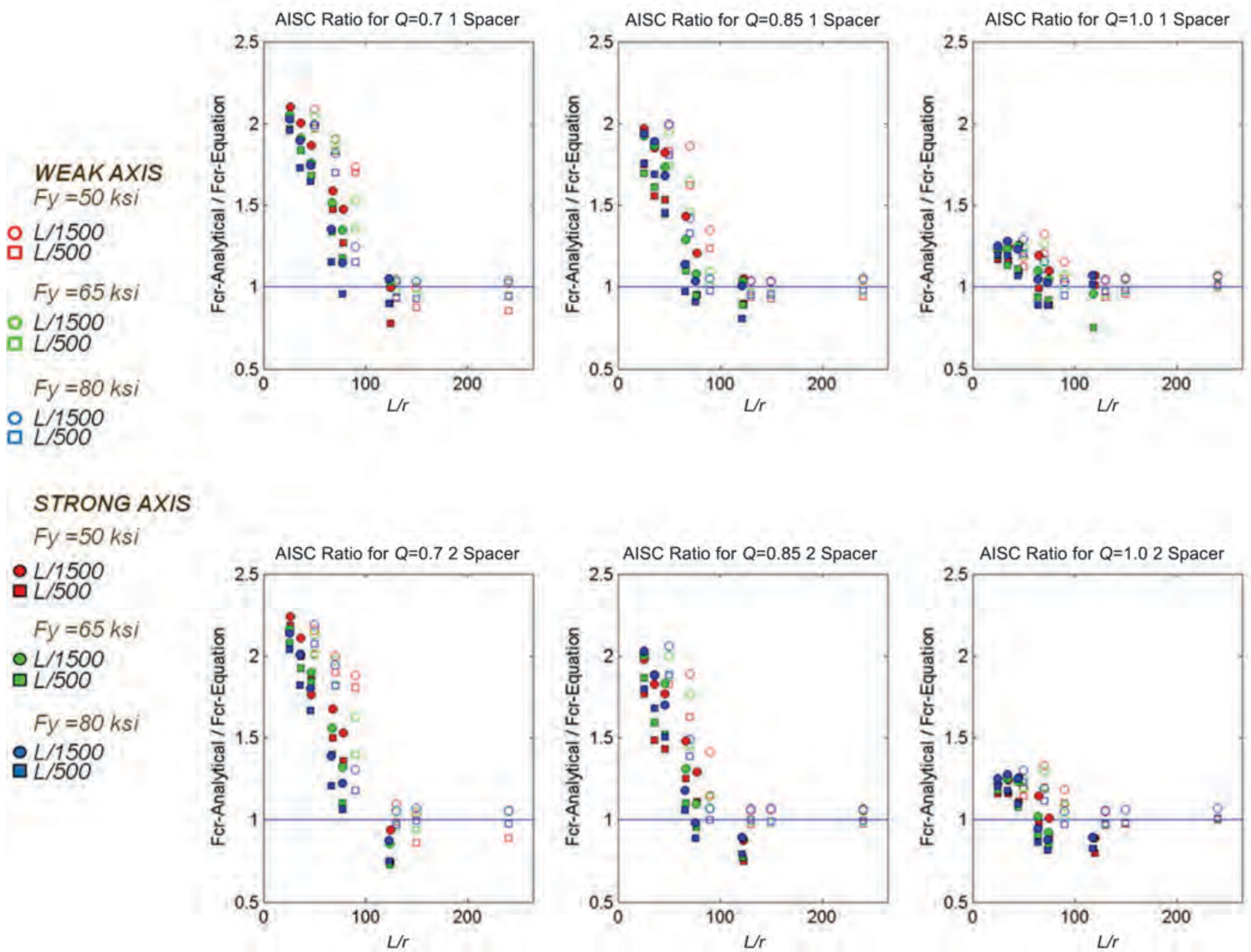

Fig. 21. LL4×4 ratios of analytical to AISC Specification *nominal strength; L/500 and L/1500 imperfection magnitudes;* F_y *= 50-, 65- and 80-ksi materials—organized per* Q *values and spacer count (compare to Fig. 15).*

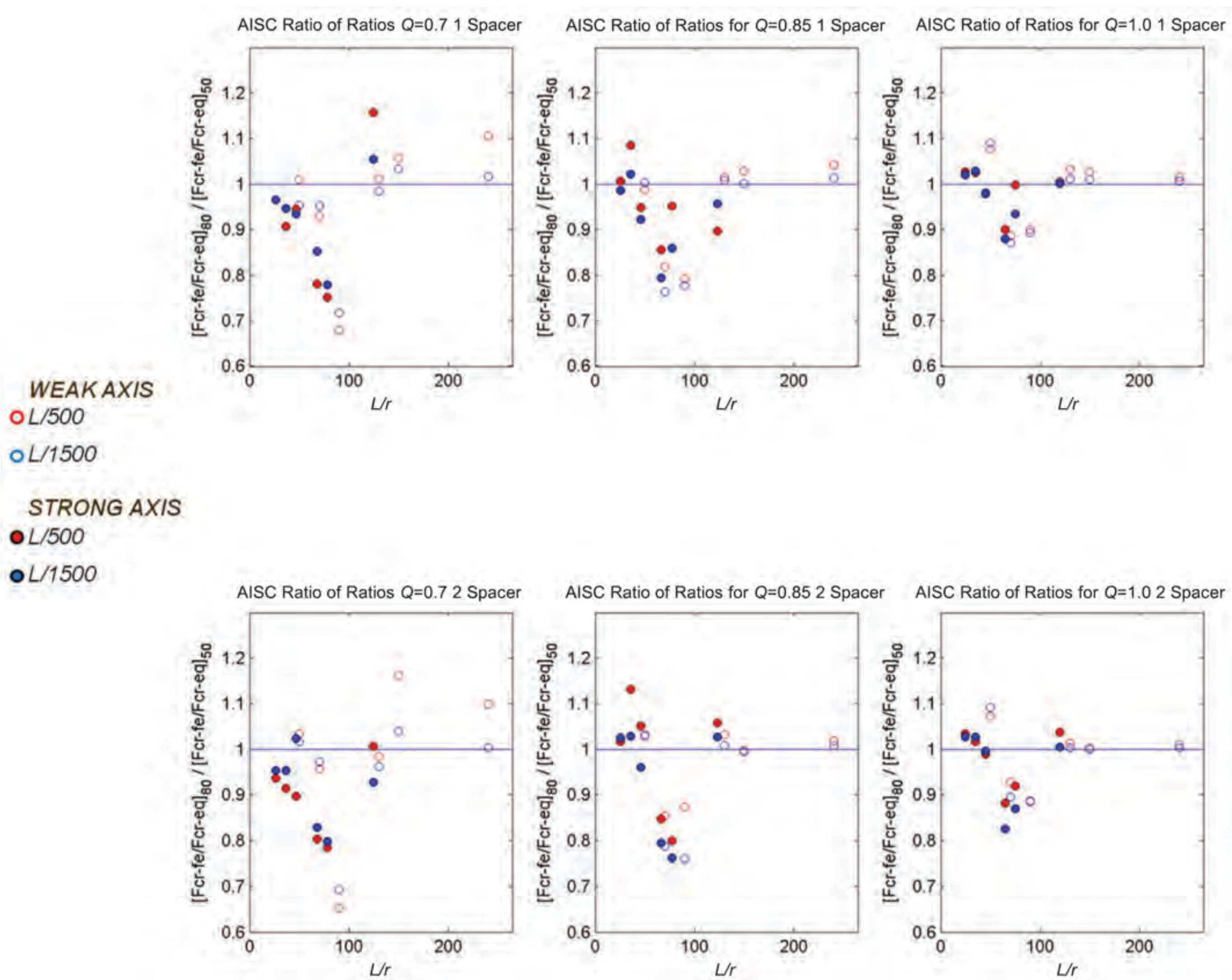

Fig. 22. LL4×4 ratio of ratios of analytical to AISC Specification *nominal strength for 80- and 50-ksi grade steel; L/500 and L/1500 imperfection magnitudes—organized per* Q *values and spacer count (compare to Fig. 16).*

Table 5. Global Comparison of Analytical to AISC *Specification* Nominal Strength Ratio of Ratios per Material Strength (compare to Table 3)								
Global Average of $(P_{fe}/P_{n}\_AISC)_{Fy}/(P_{fe}/P_{n}\_AISC)_{50}$								
		L/1500				L/500		
Axis	**Variable**	**50 ksi**	**65 ksi**	**80 ksi**		**50 ksi**	**65 ksi**	**80 ksi**
	***Q* Factor**							
Strong	0.7	1.000	0.890	0.883		1.000	0.887	0.877
	0.85	1.000	0.946	0.944		1.000	0.963	0.972
	1	1.000	0.976	0.969		1.000	0.985	0.985
Weak	0.7	1.000	0.902	0.889		1.000	0.920	0.919
	0.85	1.000	0.940	0.927		1.000	0.966	0.958
	1	1.000	0.982	0.972		1.000	0.989	0.981
	Number of Spacers							
Strong	1	1.000	0.947	0.942		1.000	0.955	0.958
	2	1.000	0.944	0.939		1.000	0.956	0.957
Weak	1	1.000	0.949	0.936		1.000	0.965	0.953
	2	1.000	0.948	0.937		1.000	0.965	0.964

Mean: Strong	1.000	0.946	0.941		1.000	0.955	0.957
Mean: Weak	1.000	0.949	0.937		1.000	0.965	0.958
Mean: Weak and strong	**1.000**	**0.947**	**0.939**		**1.000**	**0.960**	**0.958**
Grand total	**0.962**				**0.973**		

Another goal of the parametric study was to determine if modifications to the 2010 SJI buckling equations would be required for the use of HSLA-V material. Results for weak-axis buckling showed that the SJI buckling equations are adequate and appropriately conservative for almost all weak-axis buckling cases included in the study. Results for strong-axis buckling showed that the SJI buckling equations are nonconservative for many cases, and the nonconservatism increases as the Q factor decreases from 1.0 to 0.7. This nonconservatism in the strong-axis buckling equations is an issue that is independent of the steel strength.

This paper investigated the following potential solutions and their impact on resolving the observed lack of conservatism in the strong-axis buckling predictions:

- SJI adoption of all AISC provisions, including flexural-torsional buckling and a modified slenderness ratio.
- SJI adoption of only the modified slenderness ratio from the AISC *Specification*.

The use of all the AISC buckling provisions resolved the nonconservatism observed with the use of the SJI buckling equations for strong-axis bending of members with low Q factors. However, the AISC buckling equations were overly conservative and were biased against higher-strength steels. This option is not recommended for adoption.

The modified slenderness ratio in the AISC provisions significantly improved the accuracy of the SJI buckling strength predictions for strong-axis buckling cases for members with Q values less than 1.0. Furthermore, the results did not show significant bias in conservatism in relation to material strength. The authors strongly recommend that SJI consider adopting the AISC slenderness modification ratio for built-up members into the SJI Specifications. [Note: SJI adopted the modified slenderness ratio for built-up web members in its 2015 Specification (SJI, 2015).]

Additional investigation of the use of the AISC flexural-torsional buckling equations for double angles is recommended because this study suggests that these provisions produce overly conservative results in the low slenderness ratio range.

Table 6. Global Comparison of Analytical to AISC *Specification* Nominal Buckling Strength Ratios Excluding Flexural-Torsional Buckling Checks (compare to Table 2)								
Global Average of P_{fe}/P_n_AISC_NoFT_Balloted								
		L/1500				**L/500**		
Axis	**Variable**	**50 ksi**	**65 ksi**	**80 ksi**		**50 ksi**	**65 ksi**	**80 ksi**
	***Q* Factor**							
Strong	0.7	0.898	0.950	0.936		0.819	0.861	0.846
	0.85	1.091	1.094	1.089		0.949	0.969	0.976
	1	1.087	1.075	1.084		0.988	0.987	1.003
Weak	0.7	1.047	1.102	1.093		0.946	1.014	1.020
	0.85	1.185	1.172	1.161		1.065	1.083	1.081
	1	1.135	1.126	1.115		1.062	1.061	1.054
	Number of Spacers							
Strong	1	1.062	1.076	1.070		0.950	0.969	0.973
	2	1.034	1.036	1.038		0.924	0.937	0.944
Weak	1	1.124	1.127	1.116		1.030	1.051	1.043
	2	1.148	1.151	1.141		1.047	1.069	1.071

Mean: Strong	1.048	1.056	1.054	0.937	0.953	0.959
Mean: Weak	1.136	1.139	1.129	1.038	1.060	1.057
Mean: Weak and strong	**1.092**	**1.098**	**1.091**	**0.988**	**1.006**	**1.008**
Grand total	**1.094**			**1.001**		

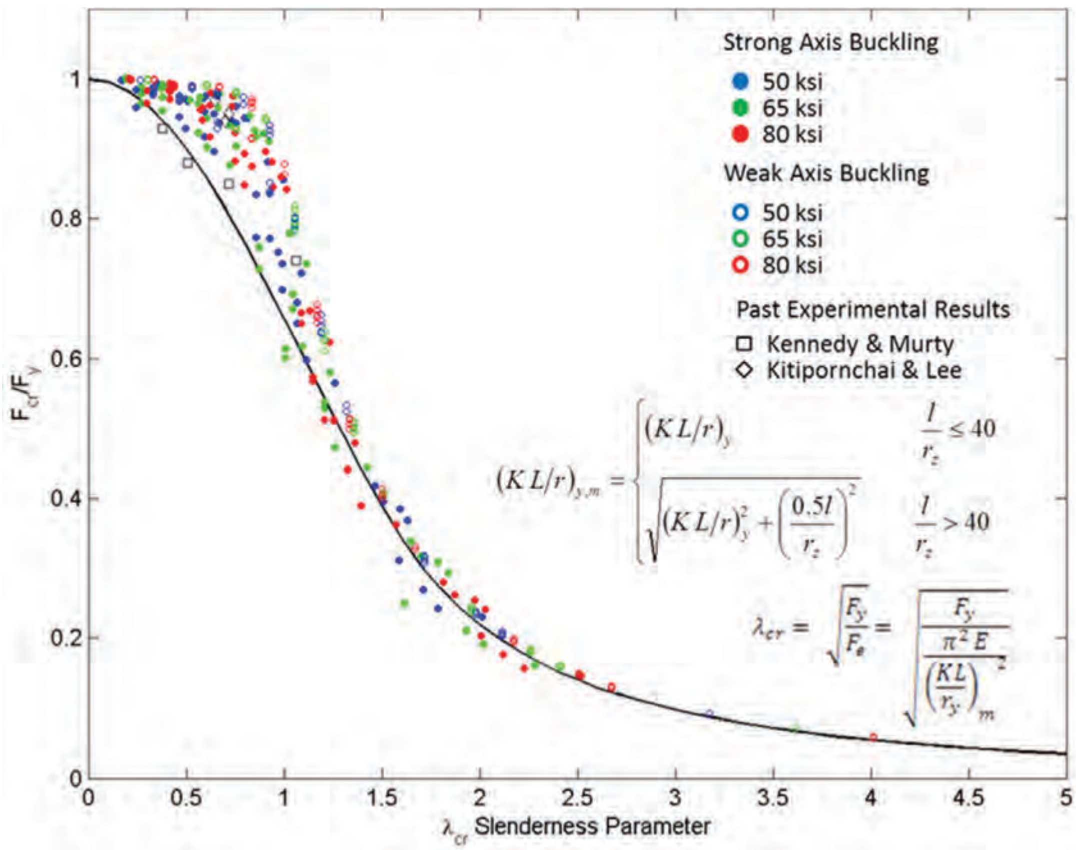

Fig. 23. Comparison of the normalized flexural buckling equation and parametric study analyses with Q = *1.0 and using the AISC slenderness modification for built-up sections.*

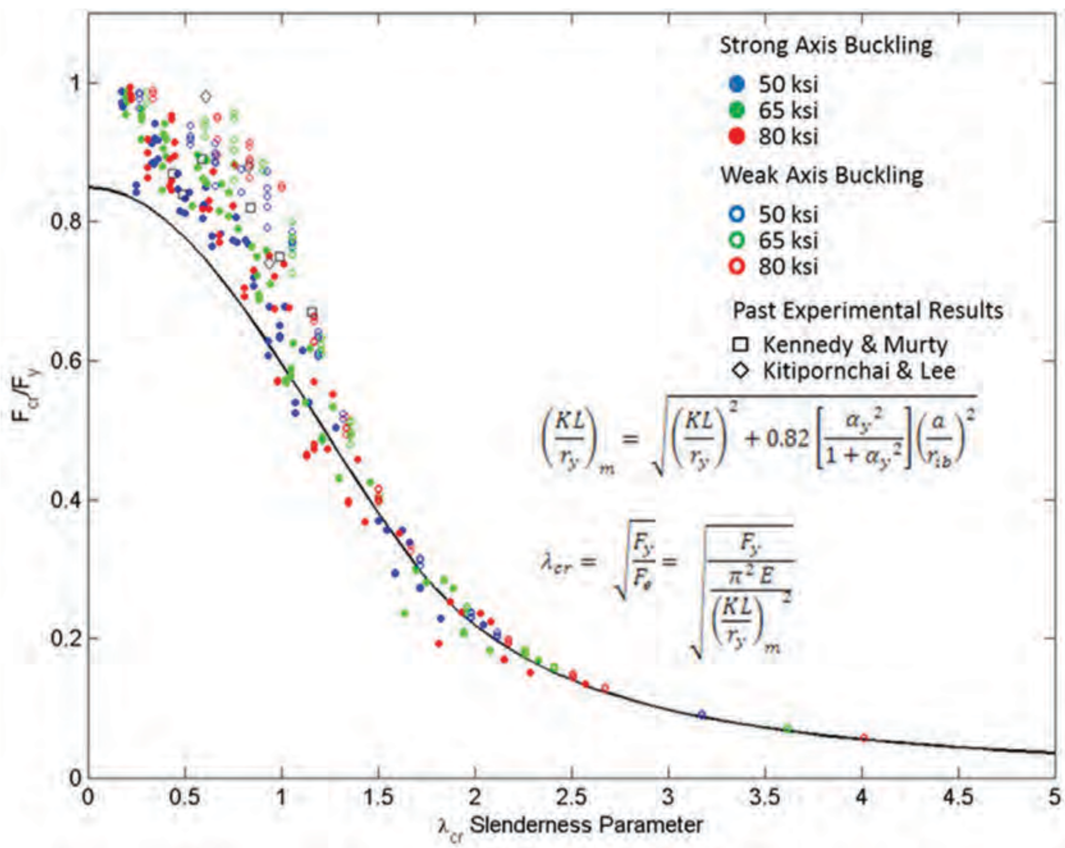

Fig. 24. Comparison of the normalized flexural buckling equation and parametric study analyses with Q = *0.85 and using the AISC slenderness modification for built-up sections.*

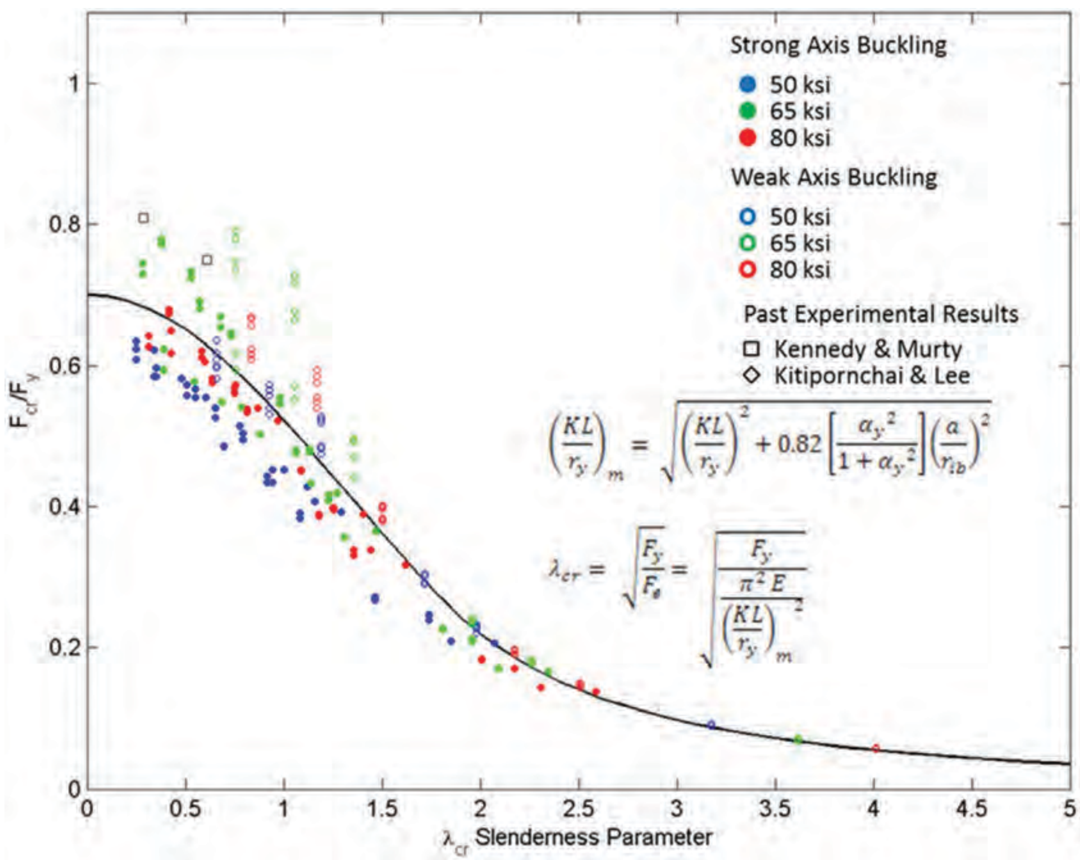

Fig. 25. Comparison of the normalized flexural buckling equation and parametric study analyses with Q = *0.7 and using the AISC slenderness modification for built-up sections.*

Table 7. Global Comparison of Analytical to AISC *Specification* Nominal Buckling Strength Ratio of Ratios Excluding Flexural-Torsional Buckling Checks (compare to Table 3)								
Global Average of $(P_{fe}/P_{n}\_AISC\_NoFT\_Bal)_{Fy}/(P_{fe}/P_{n}\_AISC\_NoFT\_Bal)_{50}$								
		L/1500				L/500		
Axis	Variable	50 ksi	65 ksi	80 ksi		50 ksi	65 ksi	80 ksi
	Q Factor							
Strong	0.7	1.000	1.059	1.043		1.000	1.056	1.037
	0.85	1.000	1.002	0.997		1.000	1.020	1.028
	1	1.000	0.989	0.999		1.000	0.997	1.015
Weak	0.7	1.000	1.053	1.045		1.000	1.074	1.080
	0.85	1.000	0.991	0.983		1.000	1.018	1.016
	1	1.000	0.994	0.986		1.000	1.000	0.994
	Number of Spacers							
Strong	1	1.000	1.015	1.009		1.000	1.022	1.025
	2	1.000	1.004	1.006		1.000	1.016	1.024
Weak	1	1.000	1.005	0.997		1.000	1.022	1.015
	2	1.000	1.005	0.998		1.000	1.024	1.027

Mean: Strong	1.000	1.009	1.007	1.000	1.019	1.025
Mean: Weak	1.000	1.005	0.997	1.000	1.023	1.021
Mean: Weak and strong	**1.000**	**1.007**	**1.002**	**1.000**	**1.021**	**1.023**
Grand total	**1.003**			**1.015**		

REFERENCES

ABAQUS (2007), *ABAQUS User's Manual*, Version 6.7, Dassault Systemes, RI.

AISC (1978), *Specification for the Design, Fabrication and Erection of Structural Steel for Buildings*, American Institute of Steel Construction, Chicago, IL.

AISC (2010), *Specification for Structural Steel Buildings*, ANSI/AISC 360, American Institute of Steel Construction, Chicago, IL.

AISI (1968), *Specifications for the Design of Cold-Formed Steel Structural Members*, American Iron and Steel Institute, Washington, DC.

Aslani, F. and Goel, S. (1991), "An Analytical Criterion for Buckling Strength of Built-up Compression Members," *Engineering Journal*, AISC, Vol. 28 No. 4.

ASTM (2007), "Standard Specification for High-Strength Low-Alloy Columbium-Vanadium Structural Steel," A572/A572M-07, ASTM International, West Conshohocken, PA.

ASTM (2008), "Standard Specification for Carbon Structural Steel," A36/A36M-08, ASTM International, West Conshohocken, PA.

Chuenmei, G. (1984), "Elastoplastic Buckling of Single Angle Columns," *Journal of Structural Engineering*, Vol. 110, No. 6, pp. 1,391–1,395.

Elgaaly, M., Dagher, H. and Davids, W. (1991), "Behavior of Single-Angle-Compression Members." *Journal of Structural Engineering*, Vol. 117, No. 12, pp. 3,720–3,741.

Elgaaly, M., Dagher, H. and Davids, W. (1992), "Non-Slender Single Angle Struts," *Engineering Journal*, AISC, Vol. 29, No. 2.

Galambos, T.V. (1991), "Design of Axially Loaded Compressed Angles," *Proceedings, 1991 Annual Technical Session, Inelastic Behavior and Design of Frames*, AISC, April 15–17.

Kennedy, J.B. and Murty, M.K.S. (1972), "Buckling of Steel Angle and Tee Struts," *Journal of the Structural Division*, ASCE, Nov.

Kennedy, J.B. and Murty, M.K.S. (1982), “Buckling of Angles: State of the Art,” *Journal of the Structural Division*, ASCE, Sept.

Kitipornchai, S. and Lee, H.W. (1986), “Inelastic Experiments on Angle and Tee Struts,” *Journal of Constructional Steel Research*, Vol. 6, pp. 219–236.

Popovic, D., Hancock, G.J. and Rasmussen, K.J.R. (1999), “Axial Compression Tests of Cold-Formed Angles,” *Journal of Structural Engineering*, ASCE, May.

Salmon, C.G. and Johnson, J.E. (1990), *Steel Structures: Design and Behavior*, 3rd Ed., Harper & Row, New York, NY.

SGH (2011), *Correlation and Sensitivity Study on the Buckling of HSLA-V Steel in Single and Double Angle Members*, Project 047079, Simpson Gumpertz and Heger Inc.

SGH (2012), *Parameter Study to Assess Modifications to the SJI Design Equations for HSLA-V Steels. Rev.1.*, Project 047079, Simpson Gumpertz and Heger Inc.

SJI (2010), *Standard Specification for Longspan Steel Joists, LH-Series and Deep Longspan Steel Joists, DLH-Series*, ANSI/SJI-LH/DLH, Steel Joist Institute, Florence, SC.

SJI (2015), *Standard Specification for K-Series, LH-Series, and DLH-Series Open Web Steel Joists and for Joist Girders*, ANSI/SJI 100, Steel Joist Institute, Florence, SC.

Talaat, M.M., Mayes, R.L., Webster, M.D., Citipitioglu, A. and Kan, F.W. (2017), “Buckling of Conventional and High-Strength Vanadium Steel Double-Angle Compression Members: Computational Parametric Evaluation of Slenderness Modification Factors.” *Engineering Journal*, AISC, Vol. 54, No. 4.

XYZ Scientific Applications (n.d.), *TrueGrid*. Livermore, CA: http://www.truegrid.com.